

TKK Dissertations 14  
Espoo 2005

## **APPLICATIONS OF MICROSTRUCTURED FIBERS**

Supercontinua and novel components

Doctoral Dissertation

**Mikko Lehtonen**



**Helsinki University of Technology**  
**Department of Electrical and Communications Engineering**  
**Optics and Molecular Materials**

TKK Dissertations 14  
Espoo 2005

## **APPLICATIONS OF MICROSTRUCTURED FIBERS**

Supercontinua and novel components

Doctoral Dissertation

**Mikko Lehtonen**

Dissertation for the degree of Doctor of Science in Technology to be presented with due permission of the Department of Electrical and Communications Engineering for public examination and debate in Micronova at Helsinki University of Technology (Espoo, Finland) on the 2nd of December, 2005, at 12 noon.

**Helsinki University of Technology  
Department of Electrical and Communications Engineering  
Optics and Molecular Materials**

**Teknillinen korkeakoulu  
Sähkö- ja tietoliikennetekniikan osasto  
Optiikka ja molekyylimateriaalit**

Distribution:

Helsinki University of Technology

Department of Electrical and Communications Engineering

Optics and Molecular Materials

P.O. Box 3500

FI - 02015 TKK

FINLAND

Tel. +358-9-4511

Fax +358-9-451 3128

URL: <http://omm.tkk.fi/>

E-mail: [mjlehton@cc.hut.fi](mailto:mjlehton@cc.hut.fi)

© 2005 Mikko Lehtonen

ISBN 951-22-7913-4

ISBN 951-22-7914-2 (PDF)

ISSN 1795-2239

ISSN 1795-4584 (PDF)

URL: <http://lib.tkk.fi/Diss/2005/isbn9512279142/>

TKK-DISS-2059

Otamedia Oy

Espoo 2005



HELSINKI UNIVERSITY OF TECHNOLOGY P.O. BOX 1000, FI-02015 TKK <a href="http://www.tkk.fi">http://www.tkk.fi</a>		ABSTRACT OF DOCTORAL DISSERTATION	
Author Mikko Juhani Lehtonen			
Name of the dissertation Applications of microstructured fibers: Supercontinua and novel components			
Date of manuscript		Date of the dissertation December 2, 2005	
<input type="checkbox"/> Monograph		<input checked="" type="checkbox"/> Article dissertation (summary + original articles)	
Department	Electrical and Communications Engineering		
Laboratory	Optics and Molecular Materials		
Field of research	Optical technology		
Opponent(s)	Anders Bjarklev, Professor		
Supervisor (Instructor)	Hanne Ludvigsen, Docent		
Abstract			
<p>Microstructured fibers are a special class of pure-silica optical fibers. They consist of a silica core, surrounded by a periodic array of air-holes running along the entire length of the fiber. These air-holes permit guidance of light through total-internal reflection. Diameter and spacing of the air-holes determines the optical properties of the fiber, therefore allowing for tailoring of the fiber according to the intended application.</p> <p>This thesis contains novel results on supercontinuum generation in microstructured fibers. Several critical advances have been made in tailoring of the fiber properties in order to further reduce power requirements hindering miniaturization of supercontinuum sources. In particular, the influence of a second zero-dispersion wavelength of the fiber and the input polarization of highly-birefringent fibers have been studied. Furthermore, a novel two-pump scheme allows for efficient generation of broadband blue-light. The generated supercontinua are applied to characterization of absorption and transmission spectra of novel optical components. The high spectral power density of supercontinuum allows for observation of several new excited-state absorption lines of Erbium-doped fibers and characterization of optical components with strong variations in the transmission spectrum.</p> <p>The second part of the thesis deals with applications developed for microstructured fibers. A tapered microstructured fiber is designed for coupling between standard fibers and photonic-crystal waveguides. An elliptical-core microstructured fiber is proposed as an efficient adapter between standard fibers and highly asymmetric waveguides. In addition, a microstructured fiber based optically bistable fiber cavity is applied to all-optical switching. In particular, an optical flip-flop is numerically studied.</p>			
Keywords microstructured fibers, supercontinuum, nonlinear optics, photonic crystals			
Number of pages	110	ISBN (printed)	951-22-7913-4
ISBN (pdf)	951-22-7914-2	ISBN (others)	
ISSN (printed)	1795-2239	ISSN (pdf)	1795-4584
Publisher	Optics and Molecular Materials, Department of Electrical and Communications Engineering		
Print distribution	Optics and Molecular Materials, Department of Electrical and Communications Engineering		
<input checked="" type="checkbox"/> The dissertation can be read at <a href="http://lib.hut.fi/Diss/2005/isbn9512279142/">http://lib.hut.fi/Diss/2005/isbn9512279142/</a>			



TEKNILLINEN KORKEAKOULU PL 1000, 02015 TTK <a href="http://www.tkk.fi">http://www.tkk.fi</a>	VÄITÖSKIRJAN TIIVISTELMÄ
Tekijä Mikko Juhani Lehtonen	
Väitöskirjan nimi Mikrorakenteisten valokuitujen sovellukset: valkoiset laserit ja uudet optiset komponentit	
Käsitteilyajan jättämispäivämäärä	Väitöstilaisuuden ajankohta 2.12.2005
<input type="checkbox"/> Monografia	<input checked="" type="checkbox"/> Yhdistelmäväitöskirja (yhteenveto + erillisartikkelit)
Osasto Sähkö- ja tietoliikennetekniikan osasto	
Laboratorio Optiikka ja molekyyli­materiaalit	
Tutkimusala Optinen teknologia	
Vastaväittäjä(t) Prof. Anders Bjarklev	
Työn valvoja Dos. Hanne Ludvigsen	
(Työn ohjaaja)	
Tiivistelmä	
<p>Mikrorakenteiset valokuidut ovat uudenlainen ryhmä valokuituja joilla on ainutlaatuisia optisia ominaisuuksia. Kuidun rakenne poikkeaa totutusta, sillä sen ydin on puhdasta kvartsilasia ja vaippa muodostuu ilmareikien muodostamasta periodisesta mikrorakenteesta, joka ohjailee valon etenemään ytimessä kuidun pituussuunnassa. Tästä valokuitujen ryhmästä tekee mielenkiintoisen nimenomaan se, että kuidun ominaisuudet määräytyvät mikrorakenteen rakenneosien, mikroskooppisen pienien ilmareikien, etäisyydestä ja halkaisijasta. Näin ollen pystytään suunnittelemaan valokuitu, jonka ominaisuudet on räätälöity käyttötarkoitusta varten, esimerkiksi siten että ytimen pinta-ala on minimoitu optisten epälineaarisuuksien maksimoimiseksi tai ytimen keskelle on muodostettu suuri ilmareikä, jota sovelletaan herkissä kaasujen absorptiomittauksissa.</p> <p>Tämä väitöskirja käsittelee mikrorakenteisia kuituja ja niiden sovelluksia epälinearisessa optiikassa ja optisten komponenttien karakterisoinnissa. Työn ensimmäisessä osiossa tutustutaan valkoisen laservalon muodostumiseen vahvasti epälinearisissa mikrorakenteisissa valokuiduissa. Lisäksi työssä esitellään uusia menetelmiä valkoisen laservalon spektrin optimoimiseksi kuidun rakennetta ja ominaisuuksia muokkaamalla. Erityisesti tutustutaan kahden syötepulssin avulla saavutettavaan merkittävään tehohyötyyn laajakaistaisen sinisen valon muodostamisessa. Työssä sovelletaan myös valkoisia laserlähteitä erilaisten optisten komponenttien karakterisointiin.</p> <p>Työn toisessa osiossa suunnitellaan ja optimoidaan lämpöohennettu mikrorakenteinen valokuitu valon tehokkaaseen kytkemiseen fotonikidevalokanavaan. Erityisesti käyttämällä elliptistä mikrorakenteista valokuitua ennustetaan saavutettavan merkittävästi parempi kytkentätehokkuus tavalliseen valokuituun verrattuna. Toisena sovelluksena tutustutaan mikrorakenteisesta valokuidusta muodostettaviin epälineaarisiiin kaviteetteihin. Eräänä sovelluksena tutkitaan optisen kiikun toteutusta epälineaarisien kaviteettien kahtaistabiilisuuden avulla.</p>	
Asiasanat fotonikidekuitu, valkoinen laservalo, fotonikiteet	
Sivumäärä 110	ISBN (painettu) 951-22-7913-4
ISBN (pdf) 951-22-7914-2	ISBN (muut)
ISSN (painettu) 1795-2239	ISSN (pdf) 1795-4584
Julkaisija Optiikka ja Molekyyli­materiaalit, Sähkö- ja tietoliikennetekniikan osasto	
Painetun väitöskirjan jakelu Optiikka ja Molekyyli­materiaalit, Sähkö- ja tietoliikennetekniikan osasto	
<input checked="" type="checkbox"/> Luettavissa verkossa osoitteessa <a href="http://lib.hut.fi/Diss/2005/isbn9512279142/">http://lib.hut.fi/Diss/2005/isbn9512279142/</a>	

## **Preface**

The work presented in this thesis has been carried out within the Fiber-Optics Group at the Metrology Research Institute of the Helsinki University of Technology. I would like to thank the Head of the Department of Electrical and Communications Engineering, Prof. Pekka Wallin, for providing the opportunity to work within the laboratory.

I am grateful to Hanne Ludvigsen for the opportunity to work within the Fiber-Optics Group and for supervision of the work. My greatest compliments go to Goëry Genty for his significant involvement to everything. His enthusiasm served as inspiration throughout my doctoral studies. Prof. Matti Kaivola is thanked for generous loan of lasers and equipment and for scientific comments on this thesis.

I would also like express my warmest gratitude to Jesse Tuominen for the great support he has given to me during all the long years. Tuomo Ritari and Tapio Niemi are thanked for keeping up the good spirit within the group. Esa Rääkkönen is acknowledged for help with the nanosecond supercontinuum. I am also very thankful for Ossi Hahtela and Ossi Kimmelma for the numerous matches of badminton we played together. Head of the Metrology Research Institute, Prof. Erkki Ikonen and Mikko Merimaa are thanked for recruiting me to work in the laboratory and for very valuable advice. Rest of the employees of the Metrology Research Institute are thanked for the unique working atmosphere they created.

Crystal Fibre A/S and NKT Research in Denmark kindly provided us with data and many of the fiber samples used in the measurements. This is acknowledged and highly valued. I am very grateful to Kaj Nyholm from Centre for Metrology and Accreditation for generous loan of the GigaOptics laser. Simo Tammela from Liekki Oy is thanked for providing high-concentration Erbium-doped fiber samples.

Academy of Finland (Future Electronics Research Programme and Project number 121117), TKK Graduate School of Information Science, Heikki- ja Hilma Honkasen säätiö, and Tekniikan Edistämissäätiö are acknowledged for financial support of the work.

I am most grateful to my family for their endless support throughout my studies. My loving and caring wife Johanna was the greatest motivator during the writing of this thesis.

Espoo, August 9, 2005

Mikko Lehtonen

# Table of contents

---

<b>ABSTRACT .....</b>	<b>I</b>
<b>PREFACE .....</b>	<b>III</b>
<b>TABLE OF CONTENTS .....</b>	<b>IV</b>
<b>LIST OF PUBLICATIONS .....</b>	<b>V</b>
<b>AUTHOR'S CONTRIBUTION.....</b>	<b>VI</b>
<b>1 INTRODUCTION.....</b>	<b>1</b>
<b>2 PHOTONIC CRYSTAL FIBERS.....</b>	<b>3</b>
2.1 CLASSES OF PHOTONIC CRYSTAL FIBERS .....	3
2.2 MODELING METHODS .....	5
2.3 PROPERTIES OF INDEX-GUIDING MICROSTRUCTURED FIBERS.....	7
<b>3 LIGHT SOURCES BASED ON MICROSTRUCTURED FIBERS.....</b>	<b>12</b>
3.1 NONLINEAR PROPAGATION IN MICROSTRUCTURED FIBERS.....	13
3.2 FUNDAMENTALS OF SUPERCONTINUUM GENERATION .....	16
3.3 ENHANCEMENT OF SUPERCONTINUUM BANDWIDTH.....	18
3.4 BROADBAND BLUE LIGHT GENERATION .....	21
<b>4 SPECTRAL CHARACTERIZATION OF OPTICAL COMPONENTS .....</b>	<b>23</b>
<b>5 OPTICAL COMPONENTS BASED ON MICROSTRUCTURED FIBERS .....</b>	<b>27</b>
5.1 TAPERED MICROSTRUCTURED FIBERS FOR COUPLING TO PHOTONIC CRYSTALS.....	27
5.2 MICROSTRUCTURED FIBER BASED SWITCH.....	30
<b>6 SUMMARY .....</b>	<b>33</b>
<b>REFERENCES .....</b>	<b>35</b>
<b>ABSTRACTS OF PUBLICATIONS .....</b>	<b>41</b>
<b>ERRATUM .....</b>	<b>43</b>

## List of publications

This thesis consists of an overview and the following selection of the author's publications:

- [P1] G. Genty, M. Lehtonen, and H. Ludvigsen, "Effect of cross-phase modulation on supercontinuum generated in microstructured fibers with sub-30 fs pulses", *Opt. Express* **12**, 4614-4624 (2004).
- [P2] G. Genty, M. Lehtonen, H. Ludvigsen, and M. Kaivola, "Enhanced bandwidth of supercontinuum generated in microstructured fibers", *Opt. Express* **12**, 3471-3480 (2004).
- [P3] M. Lehtonen, G. Genty, M. Kaivola, and H. Ludvigsen, "Supercontinuum generation in a highly birefringent microstructured fiber", *Appl. Phys. Lett.* **82**, 2197-2199 (2003).
- [P4] G. Genty, M. Lehtonen, and H. Ludvigsen, "Route to broadband blue light generation in microstructured fibers", *Opt. Lett.* **30**, 756-758 (2005).
- [P5] M. Lehtonen, G. Genty, and H. Ludvigsen, "Absorption and transmission spectral measurement of fiber-optic components using supercontinuum radiation", *Appl. Phys. B* **81**, 231-234 (2005).
- [P6] M. Lehtonen, G. Genty, and H. Ludvigsen, "Tapered microstructured fibers for efficient coupling to optical waveguides: a numerical study", *Appl. Phys. B* **81**, 295-300 (2005).
- [P7] G. Genty, M. Lehtonen, and H. Ludvigsen, "Optical bistability and signal processing in a microstructured fiber ring resonator", *Appl. Phys. B* **81**, 357-362 (2005).

## **Author's contribution**

The scientific results presented in thesis have been carried out at the Metrology Research Institute within the Fiber-Optics Group during the years 2002-2005. The thesis is composed of a short overview and seven publications referred to as [P1-P7]. These publications are the results of group effort. The author has written papers [P3,P5,P6], and contributed to the writing of all the other papers. Parts of the results of this thesis have been also presented in international conferences.

The author contributed to the experiments and development of the theory of supercontinuum generation presented in [P1-P2]. He contributed to the theory of the effect of polarization on supercontinuum generation and participated in the experiments presented in [P3]. For [P4], he was involved in the development of the theoretical model. The author performed partly the experiments presented in [P5] and the calculations and simulations shown in [P6]. For [P7] he contributed to development of the theory.

*Other related publications to which the author has contributed:*

*G. Genty, M. Lehtonen, H. Ludvigsen, J. Broeng, and M. Kaivola, "Spectral broadening of femtosecond pulses into continuum radiation in microstructured fibers", Opt. Express **10**, 1083-1098 (2002).*

# 1 Introduction

Photonic crystal fibers are a new class of optical fiber, which guide light inside their microstructured cladding [1]. The most widely used type are the microstructured fibers (MFs), which consist of a pure-silica core surrounded by a periodic array of air-holes that constitute the cladding [2]. The air-holes reduce the effective refractive index of the cladding, allowing for light to propagate in the core. The microstructure of the cladding can be varied in order to tailor the optical properties of the fiber [3]. Indeed, several fiber types have been developed, such as highly nonlinear [4], highly birefringent [5], large mode-field area [6,7] and high numerical aperture MFs [8]. Photonic bandgap fibers are a special class of photonic crystal fibers, that confine light due to a photonic bandgap of the cladding [9], allowing for guidance of light in the low-index core of the fiber. Such fibers are very promising for, e.g., sensing of gases [10].

One of the most important applications of microstructured fibers is the so-called supercontinuum (SC) generation. When highly nonlinear MFs are pumped with intense laser pulses, the spectral broadening can be so pronounced that the resulting spectrum can span more than an optical octave. Supercontinuum generation in MFs was first demonstrated in 1999 by Ranka *et al.* [11]. The physics behind the process of SC generation in MFs has recently been extensively studied, and a good understanding of the phenomena involved has been obtained [12-22]. The dominant nonlinear effects in SC generation include self-phase modulation, stimulated Raman scattering and soliton effects. Furthermore, a strong effort has been put towards developing compact and cost-efficient SC sources [23-25]. Alternative approaches to produce large-bandwidth continua have also emerged, e.g., short tapered fibers with reduced effective area and, thus, enhanced nonlinearity [26].

Supercontinuum light has the properties of a laser, i.e., it can be easily collimated to a beam or focused to a diffraction-limited spot, and its intensity can be very high. Supercontinuum light sources find numerous novel applications in, e.g., optical frequency metrology [27] and optical coherence tomography [28]. Efficient generation of coherent white light in MFs has opened up new possibilities for characterization of novel optical components. For example, SC light has already been employed in gas spectroscopy for measurements of absorption lines [29] or fluorescence imaging microscopy [30].

Photonic crystals (PCs) also in planar geometries are studied and developed for novel ways to manipulate the flow of light and they have shown great potential for many applications in the field of optics. These include low-loss waveguides with sharp bends [31], omnidirectional mirrors [32,33], inhibition of spontaneous emission [34], and various passive/active optical functions [35]. Characterization of the PCs has, however, proven to be difficult due to the poor efficiency of coupling light into these structures. Preferably the light should be brought to the PC waveguide using a fiber-

based coupling setup. The PC waveguides are usually very thin, on the order of hundreds of nanometers, to ensure pure transverse photonic bandgap guidance along the PC region. This severely limits the coupling efficiency of light from standard single-mode fibers since the dimensions of the output mode of standard fibers is quite different from the waveguide input mode. Fiber tapering provides a way to reduce the mode-field diameter of the fibers thereby allowing for a better coupling efficiency to the input of the waveguide [36,37]. In particular, tapered MFs allow for the possibility to conveniently reduce the mode-field diameter without significantly increasing the fragility or requiring very strict manufacturing tolerances.

Nonlinear fiber resonators provide convenient means for all-optical signal processing [38,39]. The high nonlinearity achieved in microstructured fibers has enabled to reduce the required lengths of fiber or input intensities. In addition, they make it possible to tailor the dispersion properties of the fiber, thus allowing for optimization of the performance of the resonator.

This thesis consists of two parts. In the first part, supercontinuum generation in microstructured fibers is studied. Effects of various pump pulse and fiber parameters on the continuum formation are analyzed in order to enhance the generated spectrum. Moreover, a two-pump technique is developed for efficient broadband blue-light generation. The second part of this work concentrates on novel applications of supercontinuum light and microstructured fibers. In particular, application of supercontinuum for characterization of novel optical components, a tapered MF as a mode-field adapter, and all-optical switching based on a MF cavity are studied.

## 2 Photonic crystal fibers

Photonic crystal fibers (PCFs) are a novel type of optical fiber exhibiting a periodic variation of the refractive index in the plane perpendicular to the direction of light propagation. The first PCFs were proposed and manufactured in the seventies [1]. However, due to limitations in the fiber manufacturing technology, the breakthrough demonstration of PCFs was reported only in 1996 [2]. Since then, fast progress has been made and several different types of fibers with a microstructure have emerged [40,41]. In this Chapter, photonic crystal fibers and their properties are discussed.

### 2.1 Classes of photonic crystal fibers

Photonic crystal fibers can be classified in two categories according to their guiding principle: index-guiding microstructured fibers (MF) which guide light in the same way as standard optical fibers, and photonic bandgap fibers (PBF) where the light is confined through the bandgap effect [9]. Common to most photonic crystal fibers is that they are fabricated by stacking glass capillary tubes inside a larger glass tube to form a preform. Other techniques reported for creating the preform include drilling and extrusion [41,42]. The preform is drawn into a hair-thin fiber after being heated to  $\sim 1900^{\circ}\text{C}$  in a fiber drawing tower.

#### *Microstructured fibers*

The core of a microstructured fiber is of fused silica and the cladding is formed by air-holes running along the entire length of the fiber. These air-holes lower the effective refractive index of the cladding with respect to the core, allowing for light to be guided inside the core by total internal reflection (see Fig. 2-1a). In such a MF, often referred to as index-guiding MF, a small fraction of light propagates in the air-holes as evanescent fields. Microstructured fibers exhibit unique optical properties compared to standard fibers. For instance, for certain sizes and arrangements of the air-holes, MFs can confine the guided light to one single mode for all wavelengths in the visible and infrared [43]. Varying the air-hole size, arrangement and symmetry also makes it possible to tailor the group-delay and thereby the dispersion properties of the fiber [44]. Narrow-core MFs have been widely applied in nonlinear optics, e.g., in supercontinuum generation and parametric amplification, due to their enhanced nonlinearity [13,45]. Large-core, endlessly single-mode MFs with high numerical aperture have been developed for applications in telecommunications and for high power delivery [46]. In particular, recent experiments have shown that it is possible to manufacture a large mode-area MF with an extremely uniform structure [47]. On the other hand, the structure can be made asymmetric in order to substantially increase the birefringence of the fiber. Highly asymmetric MFs have the advantage of maintaining the polarization state of light along propagation [5]. Several reports have also been published on fiber lasers and amplifiers that include a doped-core large mode-area

microstructured fiber (LMA-MF) [48-52]. In order to obtain a LMA-MF with high numerical aperture and large mode-area, a special design is needed, consisting of the substitution of more than one capillary with solid silica rods in the center of the preform [53]. This increases the core size while keeping the effective index of the cladding unchanged. With this type of design, output powers of several hundreds of watts from MF-based fiber lasers have been demonstrated [48].

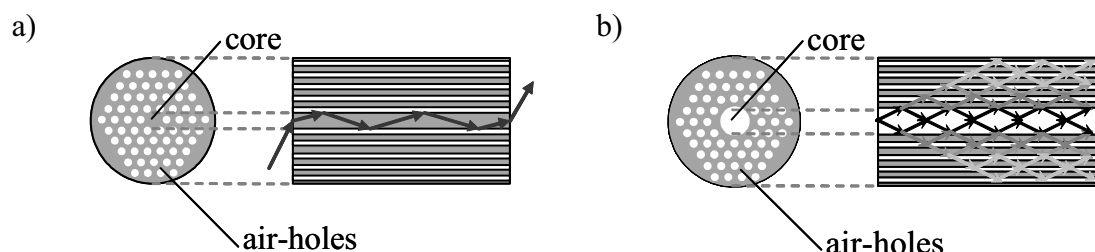


**Figure 2-1. Guidance principle of a) MF and b) PBF.**

### *Photonic bandgap fibers*

Photonic bandgap fibers differ from MFs by having a hollow core. In such a structure, index guiding is prohibited due to the lower refractive index of the core, and, therefore, PBFs guide light by consecutive constructive interferences of reflections from the several air-silica interfaces (see Fig. 2-1b). Such a periodic air-silica cladding exhibits a bandgap for photons in the radial direction, forcing the photons to propagate inside the core [9,54]. The large overlap of the propagating mode with the air core considerably lowers the nonlinearity of the fiber allowing for delivery of extremely large power levels. These fibers are also beneficial for sensing applications since a mode-field overlap larger than 98% with the air or gas in the core can be obtained compared to a few percents in index-guiding MFs [10,55]. Furthermore, bandgap fibers have high values of dispersion at the edge of the bandgap, which may be conveniently applied for dispersion compensation. Filling of the central hole of PBF with, e.g., liquid crystal material allows for formation of a new breed of in-line optical components, which may be used for example for optical switching [56].

Another type of PBF is the so-called Fresnel-fiber [41]. The Fresnel fiber uses circular symmetry whereas most other demonstrated bandgap designs exhibit hexagonal symmetry. This simplifies the design and analysis of the fiber properties. In a Fresnel-fiber, the rings of air-holes are placed at the Fresnel zones. Each ring has a Fresnel focus in the propagating direction and guidance is obtained when the foci match. The width of the bandgap can easily be tuned by simply varying the diameter of the central hole. Furthermore, the Fresnel focus of the rings can be applied in the output of the fiber to produce a small diffraction-limited spot, as with Fresnel lens [57].

## 2.2 Modeling methods

The simple structure of standard single-mode telecommunication fibers (SMFs) allows for analytical solutions of the propagating field to be calculated by solving a simple Eigenvalue equation [58]. The microstructured cladding of PCFs complicates the analysis significantly. The large refractive index contrast and strong contribution of the cladding to the waveguiding properties prevents an analytical expression for the propagating mode-field to be found. Therefore, in most cases, the mode structure and properties of PCFs are analyzed through numerical simulations. In this section, some of the numerical methods commonly applied to model the properties of PCFs are presented. Their principle characteristics are summarized in Table 1.

**Table 1. Characteristics of various methods employed for modeling MFs. MFD: mode-field diameter,  $\beta$ : propagation constant,  $A_{eff}$ : effective area,  $\lambda$ : wavelength, Pol: Polarization.**

Method	Modeled properties	Model accuracy	Limitations	Computational effort
<b>Effective-index</b>	MFD, $\beta$	Inaccurate at longer $\lambda$	Pol. analysis impossible	Low
<b>Localized function expansion</b>	MFD, $\beta$ , $A_{eff}$	Accurate	Relatively complex	High
<b>Plane-wave expansion</b>	MFD, $\beta$ , $A_{eff}$	Fair	Infinite cladding assumption	Intensive
<b>Multipole expansion</b>	MFD, $\beta$ , $A_{eff}$	Accurate	Symmetric structures	Intensive
<b>Finite-difference time domain</b>	MFD, $\beta$ , $A_{eff}$ , Propagation	Reliable	Sums over all excited modes	Very intensive
<b>Finite-difference frequency domain</b>	MFD, $\beta$ , $A_{eff}$ , Propagation	Reliable	Sums over all excited modes	High
<b>Beam propagation</b>	MFD, $\beta$ , $A_{eff}$ , Propagation	Reliable	Inefficient	High

### *Effective index method*

In the effective-index method index-guiding MFs are modeled as step-index fibers [59]. This is easiest done by taking the refractive index of the core of the equivalent step-index fiber to be that of pure silica, and determining the index of the cladding from the effective index of the so-called space-filling modes. The index of the space-filling mode is found by solving the mode that propagates if the defect is removed, i.e., if the cladding is assumed to be continuous and infinite. Knowing the propagation constant  $\beta_{SFM}$  associated with the space-filling mode, the effective refractive index of the cladding of the equivalent fiber can be deduced from

$$n_{eff}(\omega) = \frac{\beta_{SFM}(\omega)}{k_0}, \quad (2.1)$$

where  $k_0 = \omega/c$  is the wavenumber of light of angular frequency  $\omega$  propagating in free-space. The MF can then be treated as an ordinary step-index fiber. It is important to

note that the effective index method is fairly accurate only when the fundamental mode is well confined inside the core of the fiber. Nevertheless, the method permits for obtaining a quick estimate of the waveguiding properties of the fiber.

### *Expansion methods*

The most accurate way of simulating light field distribution in a waveguide is to directly apply Maxwell's equations [60]. In order to simplify the calculations, the structure or the field is often expanded into a sum of periodic functions, for which Maxwell's equations are solved. The localized functions expansion method developed for analyzing PCFs consists in expanding the electromagnetic field and the structure of the fiber into an infinite number of Hermite polynomials [61,62]. For such a field, the Maxwell's equations reduce to an algebraic Eigenvalue problem, which can be solved analytically for many types of lattices. The accuracy of the technique scales with the accuracy of the description of the refractive index profile. For this purpose, it may be necessary to use a large number of polynomials, which drastically increases the computational demands, particularly for larger and more complex structures.

In the multipole expansion method the electric field is expressed as a sum of Fourier-expansions around the individual holes of the structure [63]. The actual field is obtained from the boundary conditions on the hole surfaces. The mathematical solution of the problem is then found by solving a set of matrix equations, which limits the type of structures that can be simulated. Without symmetry, the computation time approaches infinity. Nevertheless, for symmetrical structures, the method is reasonably fast for a small number in terms of the Fourier-expansions. If more terms are needed, the method becomes computationally intensive.

The plane-wave expansion method, widely used in simulating photonic crystal structures, is based on finding the field of a periodic structure by operating in the reciprocal space, which is obtained through Fourier-transform of the lattice [9,64]. Even though in some ideal cases these solutions may be found analytically, they usually have to be obtained numerically by finding the Eigenvalues of a characteristic equation. The method is accurate and fast for two-dimensional simulations and it is particularly well suited for simulating the band structure of PBFs.

### *Finite-difference methods*

Maxwell's equations can also be applied to simulation of light propagation in waveguides. This leads to solving a number of differential equations which depend on space and time. Two most general ways of doing this are the finite-difference time domain and frequency domain methods [65,66]. Both techniques discretize the modeled structure into homogenous cells, for which Maxwell's equations are solved in a differentiated form. In the time domain method, the discretization of the equations is done in time space, and in the frequency domain method in frequency space. Both methods are well adapted for simulating PCFs, but the result of the

computation produces a sum of all propagating modes, and therefore individual modes cannot be distinguished.

### *Beam propagation method*

Finite-difference beam-propagation method (BPM) is a propagation algorithm, in which the field in the transverse plane is divided into discrete cells and the propagation is done in short steps. For each simulation step, a set of equations derived from the Maxwell's equations are solved to produce the input field for the following step [67]. This is repeated along the entire length of the structure. The beam-propagation method can be extended to 3D simulations by using the alternating direction implicit method [68]. The addition of polarization to the simulation requires taking the vectorial nature of the electric field into account. In this case, the propagation is performed by solving two coupled differential equations, one corresponding to each basis polarization state.

The beam propagation method can be conveniently extended to solve the various modes that can propagate in a 3D structure (i.e., in a  $z$ -invariant geometry). Propagation in such a structure can equivalently be described in terms of modes and propagation constants. For scalar fields, this corresponds to expressing the input field  $E(x,y,z)$  as a superposition of the Eigenmodes of the structure

$$E(x, y, z) = \sum_i \alpha_i E_i(x, y), \quad (2.2)$$

where  $\alpha_i$  represents the contribution of each mode  $E_i(x,y)$ . The input field is subsequently inserted into the BPM algorithm with the exception that the distance  $z$  is replaced by an imaginary distance  $iz$  [69]. As a consequence, along propagation, the constant  $\alpha_i$  of the fundamental mode (the mode with the highest mode index) will grow exponentially, dominating over all the other modes. Therefore, after a certain distance  $z$ , only the mode pattern of the fundamental mode is retained. Higher-order modes can also be obtained by repeating the propagation operation and suppressing the modes of lower order than the one of interest from the input field.

## **2.3 Properties of index-guiding microstructured fibers**

### *Modal behavior*

The number of modes supported by a MF depends strongly on the hole diameter  $d$ , pitch  $A$  and wavelength  $\lambda$ . Similarly to standard fibers, one can using the effective-index model define the  $V$ -parameter of MFs, known as the normalized frequency of the fiber

$$V = \frac{2\pi\rho}{\lambda} \sqrt{n_{core}^2 - n_{cladding}^2}, \quad (2.3)$$

where  $\rho$  is the effective core radius of the fiber, and  $n_{core}$  and  $n_{cladding}$  represent the refractive indices of the core and cladding, respectively [58]. The effective core radius is commonly approximated to be 0.62 times the radius of the silica core [70]. The refractive index of the core is that of silica, and the index of the cladding is the effective index of the space-filling mode. The  $V$ -parameter relates to the number of modes supported by the fiber. In particular, for values of  $V < 4.2$ , only the fundamental mode will propagate along the MF, which is often desired in telecommunication applications as multi-mode propagation induces temporal broadening of light pulses (note that in standard fibers the single-mode cutoff is  $V = 2.405$ ). Examples of  $V$ -parameters calculated for MFs as a function of normalized wavelength  $\Lambda/\lambda$  are illustrated in Fig. 2-2 for different values of the hole diameter to pitch ratio  $d/\Lambda$ .

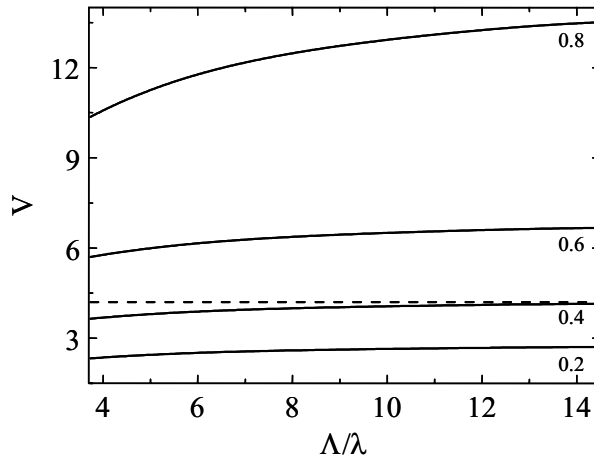


**Figure 2-2.** Calculated  $V$ -parameter of microstructured fibers for different values of  $d/\Lambda$ .  $\Lambda = 7 \mu\text{m}$ . The dashed horizontal line indicates the higher-order mode cutoff.

Contrarily to the standard step-index fibers, the refractive index of the microstructure cladding is wavelength-dependent. This can be used for reducing the wavelength-dependence of the  $V$ -parameter and thereby shortening the cutoff wavelength. For MFs with a relative air-hole diameter  $d/\Lambda$  smaller than  $\sim 0.48$ , the  $V$ -parameter shows single-mode propagation from 400 to 1600 nm [43]. Such MFs are commonly referred to as endlessly single-mode fibers and are of particular interest in, e.g., supercontinuum experiments where ultra-broadband coherent light can be generated in a single-mode. Microstructured fibers with the relative air-hole diameter larger than  $\sim 0.48$  are multi-mode. Distribution of the input light into the modes of the MF is determined by the input coupling conditions. Examples of simulated intensity profiles of the fundamental and a higher-order mode propagating in a multi-mode MF ( $\Lambda = 7 \mu\text{m}$ ,  $d/\Lambda = 0.5$ ) for  $\lambda = 800 \text{ nm}$  are presented in Fig. 2-3.

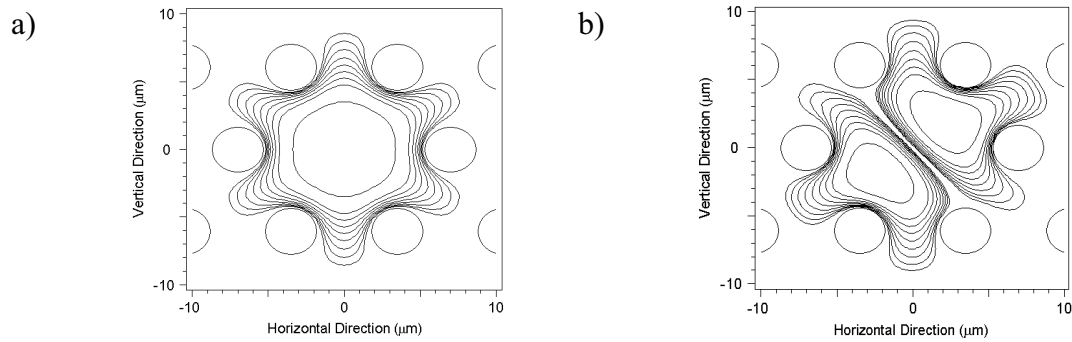


**Figure 2-3.** Intensity profile of the a) fundamental, and b) first higher-order mode of a MF with  $d=0.5 \mu\text{m}$  and  $\Lambda=7 \mu\text{m}$  simulated using the BPM method. The contour-lines are spaced by 0.5 dB.  $\lambda=800 \text{ nm}$ .

The nonlinearity of the fiber is inversely proportional to the effective area of the mode. Therefore, nonlinear MFs have very narrow cores, and thus, small values of the mode-field diameter (MFD). The MFD of MFs is strongly dependent on the relative air-hole diameter as shown in Fig. 2-4 for a fundamental mode of a triangular lattice of circular holes at  $\lambda=1500 \text{ nm}$  [71]. The tendency of the MFD to increase for small values of  $\Lambda$  and  $d/\Lambda$  can be explained as leaking of the mode into the cladding through the silica bridges in the cladding microstructure. For this reason, most fibers designed to have small MFD have very high values of  $d/\Lambda$ . As the outcome, these fibers are multi-mode, but with careful coupling of the pump light into the fiber single-mode guidance may be obtained for short lengths of fiber.

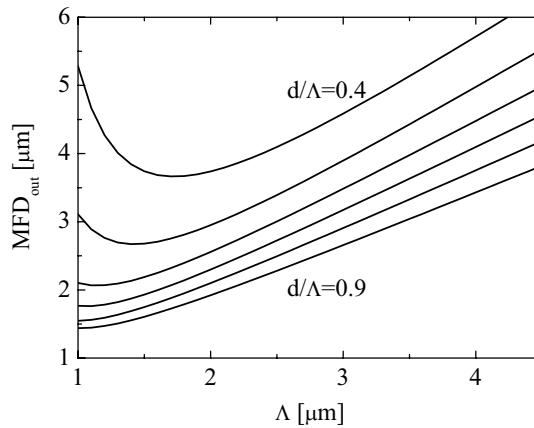


**Figure 2-4.** Calculated relation between pitch and output mode-field diameter of MFs with triangular array of circular holes for different values of the relative air-hole diameter  $d/\Lambda$ .  $\lambda=1.5 \mu\text{m}$ .

### Dispersion

Frequency-dependence of the refractive index of silica, i.e., dependence of the propagation velocity on frequency, is commonly referred to as material dispersion. The difference in the refractive index between the core and cladding induces another type of dispersion known as waveguide dispersion. The total dispersion of the fiber is the sum of the material and waveguide dispersion [72]. The effects of dispersion on

pulse propagation in optical fibers are typically accounted for by expanding the propagation constant  $\beta$  into a power series around the carrier frequency  $\omega_0$  of the pulse:

$$\beta(\omega) = \sum_{m=1}^{+\infty} \frac{\beta_m (\omega - \omega_0)^m}{m!}, \quad (2.4)$$

where

$$\beta_m = \left. \frac{d^m \beta}{d\omega^m} \right|_{\omega=\omega_0}. \quad (2.5)$$

In Eq. (2.4) the coefficient  $\beta_1$  indicates the group delay (GD) and its inverse  $\beta_1^{-1}$  the group velocity (GV) of the pulse, i.e., the propagation speed of the pulse envelope inside the fiber. The group-velocity dispersion (GVD) parameter  $\beta_2$  expresses that different frequency components of the pulse propagate at different speeds. This effect is responsible for broadening of the time intensity profile of a pulse during propagation along the fiber. Depending on its sign the group-velocity dispersion in optical fibers can be divided into two categories: it is called normal, when  $\beta_2 > 0$  and anomalous, when  $\beta_2 < 0$ . The wavelength at which  $\beta_2 = 0$  is referred to as the zero-dispersion wavelength  $\lambda_{ZD}$  ( $\lambda_{ZD} \approx 1.3 \mu\text{m}$  for conventional optical fibers). In the anomalous dispersion region, shorter wavelengths travel faster than longer wavelengths, and vice-versa in the region of normal dispersion. Another common parameter used to describe the effects of dispersion in optical fibers is the dispersion parameter  $D$  defined as

$$D = - \left( \frac{2\pi c}{\lambda^2} \right) \beta_2, \quad (2.6)$$

where  $\lambda$  is the wavelength and  $c$  the speed of light in vacuum. The value of  $D$  is often given in units of ps/(nm·km).

In MFs, the effective index of refraction of the cladding and of the core are determined by the pitch  $\Lambda$  and the relative air-hole diameter  $d/\Lambda$  of the structure [73]. Therefore, varying the characteristic dimensions of the fiber permits tailoring of the waveguide dispersion in a wide range. For comparison, the dispersion profile of a conventional single-mode telecommunication fiber (SMF) and that of several MF designs for different values of  $d/\Lambda$  are plotted in Fig. 2-5. The dispersion profiles of the MFs were calculated using the effective-index method. For large values of  $d/\Lambda$ , the effective refractive index of the cladding is close to 1. This induces higher values for the waveguide dispersion compared to conventional fibers, resulting in the shift of the  $\lambda_{ZD}$  to the visible, followed by the emerging of a second, infrared  $\lambda_{ZD}$ . This type of dispersion profile is particularly suitable for efficient supercontinuum generation, and it is further discussed in Chapter 3.

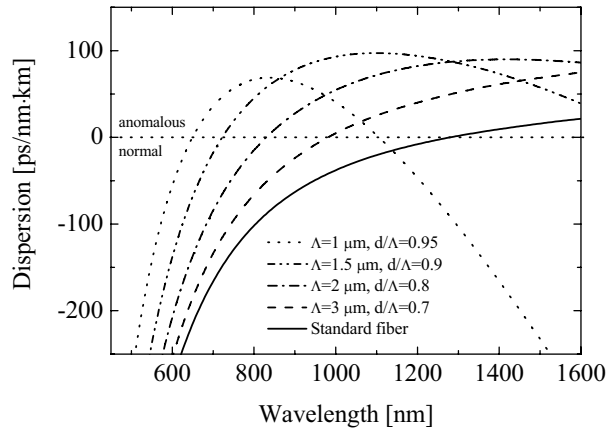


**Figure 2-5. Calculated dispersion profile of SMF and several MFs for different values of  $\Lambda$  and  $d/\Lambda$ .**

### *Attenuation*

The usable wavelength range of MFs is limited by both the intrinsic material losses and micro/macro-bending losses of the fiber. The main loss mechanisms in MFs originate from scattering and absorption [46]. Rayleigh scattering is the main loss mechanism in the wavelength range of 500-1600 nm with a cross-section proportional to  $\lambda^{-4}$ . Below 500 nm, the ultraviolet absorption of silica becomes dominant. At wavelengths above 1600 nm, the transmission of the fiber is limited by the strong infrared absorption of silica. A strong absorption peak is located at around 1400 nm resulting from vibrational resonance of the OH-molecules that remain in the fiber after the manufacturing process. In order to reduce the OH-losses, the fiber preform can be flushed with an inert gas or liquid before the drawing. In practice, losses of MFs may be reduced below 1 dB/km at 1550 nm. Further advances are theoretically possible with air-guiding photonic bandgap fibers, since Rayleigh scattering is negligible in these.

In addition to scattering and absorption, the transmission bandwidth of MFs is also limited by micro-and macro-bending losses. Macro-bending losses present in MFs are induced by bending or spooling of the fiber to a small diameter [74]. Spooling of a large mode-field area MF to a radius of 8 cm reduces the bandwidth significantly by introducing spatial asymmetry into the effective index of the cladding. Micro-deformation-induced losses are caused by scattering from interfaces of small irregularities of the fiber or by residual stress of the coating [75]. These two loss mechanisms severely limit the usable bandwidth to a few hundred nanometers for fibers with small values of the relative air-hole diameter.

### 3 Light sources based on microstructured fibers

The first observation of the dramatic broadening of ultrashort pulses into a supercontinuum (SC) was made in 1970 when pulses from a high-power Nd:glass-laser were targeted into a piece of borosilicate glass [76]. Since then, this effect has been studied extensively in several materials using free-space optics and a wide variety of laser sources (see, e.g., [77,78]). Parameters of some of the demonstrated SC sources are summarized in Table 2. The field of nonlinear fiber-optics began to evolve rapidly in the 1980s as the long effective interaction length provided by low-loss optical fibers significantly reduced the required power levels to generate SC. Indeed, already in 1987 SC generation was demonstrated in a multi-mode fiber [79]. Subsequent research concentrated on designing fibers with dispersion profiles tailored for obtaining broader SC spectra [80]. Supercontinuum generation was also demonstrated in tapered standard fibers with reduced mode-field diameters, and, thereby, enhanced nonlinearity [26]. Highly nonlinear MFs with the zero-dispersion wavelength  $\lambda_{ZD}$  in the visible were introduced in 1999 [81]. These fibers could conveniently be pumped with a mode-locked Ti:Sapphire laser, which provides femtosecond pulses with tens of kilowatts of peak power at a wavelength in the 700-1000 nm range. When launched into a highly nonlinear MF with anomalous dispersion at the pump wavelength  $\lambda_P$ , these pulses evolve into a SC that can span more than an optical octave [11]. Such intense coherent broadband radiation has several applications, e.g., in the fields of optical frequency metrology and spectroscopy [82]. The mechanisms behind SC generation in MFs have been found to strongly depend on the choice of the fiber and the pump laser [13-15,18]. Since the work by *Ranka et al.*, SC generation in MFs has been extensively studied for various pumping schemes. Continuum in MFs made of specialty glass have also been obtained [42,83]. The use of pico- and nanosecond pump pulses generated by compact and cost-efficient lasers recently been demonstrated [84].

**Table 2.** Comparison of supercontinuum sources. MMF=Multi-mode fiber, DSF=Dispersion-shifted fiber, MF=Microstructured fiber.

Year	Medium	Pump laser	Pump intensity / Peak power	SC -20 dB bandwidth
1970 [76]	Borosilicate	Nd:Glass	1 GW/cm <sup>2</sup>	300 nm
1977 [77]	Water	YAIG:Nd	45 MW	600 nm
1983 [78]	Ethylene glycol	Rh6G dye laser	3 GW	130 nm
1987 [79]	MMF	Nd:YAG	1.5 GW/cm <sup>2</sup>	60 nm
1995 [80]	DSF	Er <sup>3+</sup> fiber laser	1.2 kW	300 nm
1999 [11]	MF	Ti:Sapphire	8 kW	1200 nm

In the first section of this Chapter, basics of nonlinear fiber optics are briefly introduced. The second section highlights the steps leading to SC generation in MFs for different pump sources and dispersion characteristics of the fiber at the pump

wavelength. Enhancement of the SC bandwidth with optimized fiber designs is discussed in Chapter 3.3. A novel concept for broadband blue light generation with average pump power of only a fraction of that needed for SC generation are presented in the final section of this Chapter.

### 3.1 Nonlinear propagation in microstructured fibers

Propagation of an electromagnetic wave in a waveguide can be described by the scalar wave equation [72]

$$\nabla^2 E - \frac{1}{c^2} \frac{\partial^2 E}{\partial t^2} = -\mu_0 \frac{\partial^2 P}{\partial t^2}, \quad (3.1)$$

where  $E$  is the electric field,  $P$  is the polarization induced in the medium by the electric field,  $\mu_0$  is the permittivity of vacuum, and  $c$  is the speed of light in vacuum. Weak electric fields induce a linear polarization  $P$ . For more intense laser radiation, the polarization is composed of a linear part and an intensity dependent nonlinear part as

$$P = \varepsilon_0 \left( \chi^{(1)} E + \chi^{(2)} E^2 + \chi^{(3)} E^3 + \dots \right), \quad (3.2)$$

where  $\varepsilon_0$  is the vacuum permittivity, and  $\chi^{(j)}$  describes the  $j^{\text{th}}$  order susceptibility of the medium. In silica, due to the inversion-symmetry of the lattice crystal, the even-order susceptibilities are negligible. Moreover, susceptibilities of order higher than three are typically very low and thus insignificant. Therefore, most nonlinear effects present in silica fibers are induced by  $\chi^{(3)}$  [72]. These effects include elastic processes such as self-phase modulation (SPM) [85], cross-phase modulation (XPM) [72,86], four-wave mixing (FWM) [87], self-steepening [88], third-harmonic generation, and inelastic nonlinear scattering mechanisms, such as Raman [89,90], and Brillouin scatterings. In practice third-harmonic generation is relatively inefficient in optical fibers due to the required strict phase-matching condition. Brillouin scattering is negligible for sub-nanosecond pulses. Therefore, these two effects are not discussed further in this work.

Assuming an electric field of the form

$$E(z, T) = A(z, T) e^{-i(\beta z - \omega_0 t)}, \quad (3.3)$$

where  $A$  is the slowly varying envelope of the field and  $\beta$  represents the propagation constant of the mode at the carrier frequency  $\omega_0$ , and using the perturbation theory in Eq. (3.1) with the polarization  $P$  given by Eq. (3.2), one can derive the well-known nonlinear Schrödinger equation (NSE) which describes pulse propagation in the fiber. In a frame of reference moving at the group velocity of the pulse the NSE can be expressed as [72]

$$\frac{\partial A}{\partial z} + \frac{\alpha}{2} z - \sum_{k \geq 2} i^{k+1} \frac{\beta_k}{k!} \frac{\partial^k A}{\partial T^k} = i\gamma \left( 1 + \frac{i}{\omega_0} \frac{\partial}{\partial T} \right) \left[ A(z, T) \int_0^\infty R(T') |A(z, T - T')|^2 dT' \right]. \quad (3.4)$$

Here  $\alpha$  is the fiber loss,  $\beta_k$  are the coefficients of the Taylor-series expansion of the propagation constant  $\beta$  around  $\omega_0$ , and  $\gamma$  is the nonlinearity of the fiber. The parameter  $R(T) = (1-f_R) \cdot \delta T + f_R h_R(T)$  represents the nonlinear response function of the fiber, where  $f_R$  is the fractional contribution of the delayed response  $h_R$  induced by Raman scattering and is taken to be 0.18 for silica fibers. The Dirac function  $\delta T$  expresses the instantaneous response of the medium and is responsible for effects such as SPM, XPM and FWM. The left-hand side of the equation accounts for linear effects, such as attenuation and dispersion, and the right-hand side represents the nonlinear effects.

### *Solitonic effects*

Equation (3.4) has no analytical solution in its full form. However, when neglecting the higher-order dispersion terms (i.e., the terms with  $\beta_k$ ,  $k \geq 3$ ) and attenuation, and assuming a pure instantaneous response, it can be expressed as

$$i \frac{\partial A}{\partial z} = \frac{1}{2} \text{sgn}(\beta_2) \frac{\partial^2 A}{\partial T^2} - N^2 A |A|^2, \quad (3.5)$$

where  $\text{sgn}$  refers to the sign function and  $N$  is defined as

$$N = \sqrt{\frac{L_D}{L_{NL}}} = \sqrt{\frac{\gamma P_P T_0^2}{|\beta_2|}}. \quad (3.6)$$

Here  $L_D = T_0^2 / |\beta_2|$  and  $L_{NL} = 1 / \gamma P_P$  define the dispersion and nonlinear lengths, respectively. The parameter  $T_0 = T_{FWHM} / 1.76$  is the temporal width of the pulse ( $T_{FWHM}$  is the full width at half maximum of the pulse). Equation (3.5) has analytical solutions (commonly referred to as optical solitons) for negative values of  $\beta_2$ , i.e., when the dispersion is anomalous [72,91,92]. These solutions can be sought for using the inverse scattering method [93]. A particular solution to the equation is the so-called solitary wave which may be expressed as

$$A(T, z = 0) = N \cdot \text{sech} \left( \frac{T}{T_0} \right), \quad (3.7)$$

where the integer value closest to  $N$  is the soliton order. The solution with  $N=1$  represents the fundamental soliton, i.e., a state where the effects of anomalous dispersion and SPM cancel out, allowing for the pulse to propagate in the medium undistorted. For values of  $N$  higher than 1, the energy of the input pulse is divided between  $N$  fundamental solitons so that the peak power and duration of the  $k^{\text{th}}$  pulse ( $k \leq N$ ) are given by [94,95]

$$P_k = \frac{(2N - 2k + 1)^2}{N^2} P_P, \quad (3.8)$$

$$T_k = \frac{T_0}{2N - 2k + 1}. \quad (3.9)$$

The group velocities of the fundamental solitons that constitute a higher-order soliton are equal, and thus the pulses propagate together. No energy is exchanged between the pulses. Moreover, these sub-pulses interfere along propagation, resulting in a periodic evolution of the time trace, with the soliton period given by  $L_D \cdot \pi/2$  [72]. A higher-order soliton is, however, not stable. Even a small perturbation can break the degeneracy of the group velocities of the  $N$  constituents, leading to subsequent separation of the constituents. Examples of such perturbations include stimulated Raman scattering, self-steepening, or higher-order dispersion [94-96].

The Raman gain significantly overlaps the pulse spectrum of a femtosecond soliton. As a consequence, the leading edge of the soliton corresponding to the blue part of the spectrum acts as a pump for the trailing edge of the pulse corresponding to the red side, thus shifting the center wavelength of the pulse towards longer wavelengths [97]. This effect is known as the soliton self-frequency shift (SSFS) and the magnitude of the shift is proportional to  $1/T_0^4$ . When a soliton experiences loss, it reshapes to compensate for the lost peak power, i.e., its width increases. Therefore, even a small loss significantly reduces the SSFS. Eventually, the SSFS process ends when the Raman gain does not overlap anymore with the pulse spectrum. Theoretically, this effect is not limited solely to solitons. Indeed, it was recently predicted that Raman-induced frequency shift should also occur for Gaussian pulses in the normal-dispersion region [98]. However, the effect is in this case very inefficient due to the rapid temporal broadening of the pulse by dispersion.

The wave-number of a soliton is constant throughout the pulse spectrum. Therefore, a possibility exists for a resonance between a soliton and a linear dispersive wave (DW), whose center wavelength lies in the normal dispersion region. This possibility can be expressed through a phase-matching condition as

$$\Delta\beta = \beta(\omega_P) - \beta(\omega_{DW}) = (1 - f_r) \gamma(\omega_P) P_P - \sum_{n \geq 2} \frac{(\omega_{DW} - \omega_P)^n}{n!} \beta_n(\omega_P) = 0. \quad (3.10)$$

Here  $\omega_P$  and  $\omega_{DW}$  refer to the frequencies of the soliton and the dispersive waves, respectively. If the pulse spectrum of the soliton overlaps with the resonance, the overlapping part of the soliton spectrum is then shed into the DW [99]. The magnitude of the energy flow is determined by the overlap of the soliton spectrum and the resonance [100]. If, for example, the soliton loses energy from the blue side the spectrum to the DW, the energy within the soliton is redistributed and the net result is a red shift of its spectrum. This in turn reduces the overlap with the DW and eventually the energy transfer between the two waves ceases.

### 3.2 Fundamentals of supercontinuum generation

The sequence of events in supercontinuum generation depends strongly on the parameters of the pump pulse and the fiber characteristics. The most significant parameter is the dispersion at  $\lambda_P$  (anomalous or normal). Furthermore, the relative importance of the effects is different for femtosecond and pico/nanosecond pump pulses. Therefore, the spectrum can be tailored by a proper choice of the pump laser and the fiber.

In Fig. 3-1 spectra generated in three different MFs are plotted. The supercontinuum shown in Fig. 3-1a was generated by launching the 80 MHz train of 100 fs pulses from a mode-locked Ti:Sapphire laser into a 75 cm long MF with anomalous dispersion at the pump wavelength  $\lambda_P=800$  nm. The 2- $\mu\text{m}$  core MF possesses a zero-dispersion wavelength  $\lambda_{ZD}$  at around 760 nm. With 100 mW of input power the SC spectrum spans from 500 to 1600 nm. Figure 3-1b shows the spectrum recorded when the same pulse-train was launched into a MF with  $\lambda_{ZD}=940$  nm and normal-dispersion at  $\lambda_P$ . Supercontinuum shown in Fig. 3-1c was generated by launching pulses at a repetition rate of 30 kHz obtained from a diode-pumped Q-switched Nd:YAG laser into a 20 m long MF with anomalous dispersion at  $\lambda_P$ . This laser produces nanosecond pulses with a maximum average power of 180 mW at 1064 nm. The core size of the MF is 4.8  $\mu\text{m}$  yielding a zero-dispersion wavelength located at around 1040 nm. From Fig. 3-1 it is clear that the SC spectrum can vary substantially depending on the initial pump pulse parameters. In the following paragraphs the mechanisms leading to the formation of SC in these cases will be addressed by presenting simulation results obtained by solving Eq. (3.4) numerically using a standard split-step algorithm.

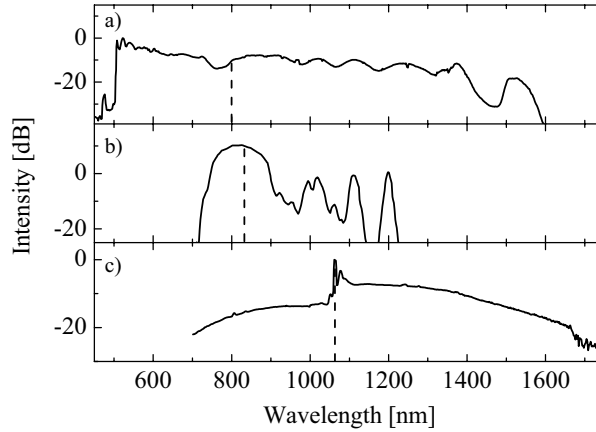


**Figure 3-1.** Measured spectra of the fs supercontinuum with  $\lambda_P$  in the a) anomalous and b) normal dispersion region. c) Supercontinuum generated with ns pump pulses and  $\lambda_P$  in the anomalous dispersion region. The dashed vertical lines mark  $\lambda_P$ .

#### *Supercontinuum generation with femtosecond pump pulses*

Supercontinuum generation with femtosecond pump pulses and anomalous dispersion at the pump wavelength is initiated by decay of a higher order soliton [12,13,16,19]. The Gaussian input pulse ( $\lambda_P=800$  nm,  $\lambda_{ZD}\approx 690$  nm,  $P_{av}=60$  mW,  $T_{FWHM}=200$  fs),

containing energy sufficient to form a higher-order soliton, splits into the constituents of different durations  $T_k$  and peak powers  $P_k$  given by Eqs. (3.8) and (3.9). Spectra of the narrowest solitons then extend to the normal-dispersion region (the extension being enhanced by self-steepening) and fulfill the phase-matching condition of Eq. (3.10), therefore resulting in the generation of DWs in the blue wavelength side (Fig. 3-2a). Subsequently, each of the solitons experiences the SSFS, which extends the SC spectrum towards red wavelengths (see Fig. 3-2b) [13]. The rate of the frequency shift is different for each soliton due to the difference in the initial pulse constituents parameters.

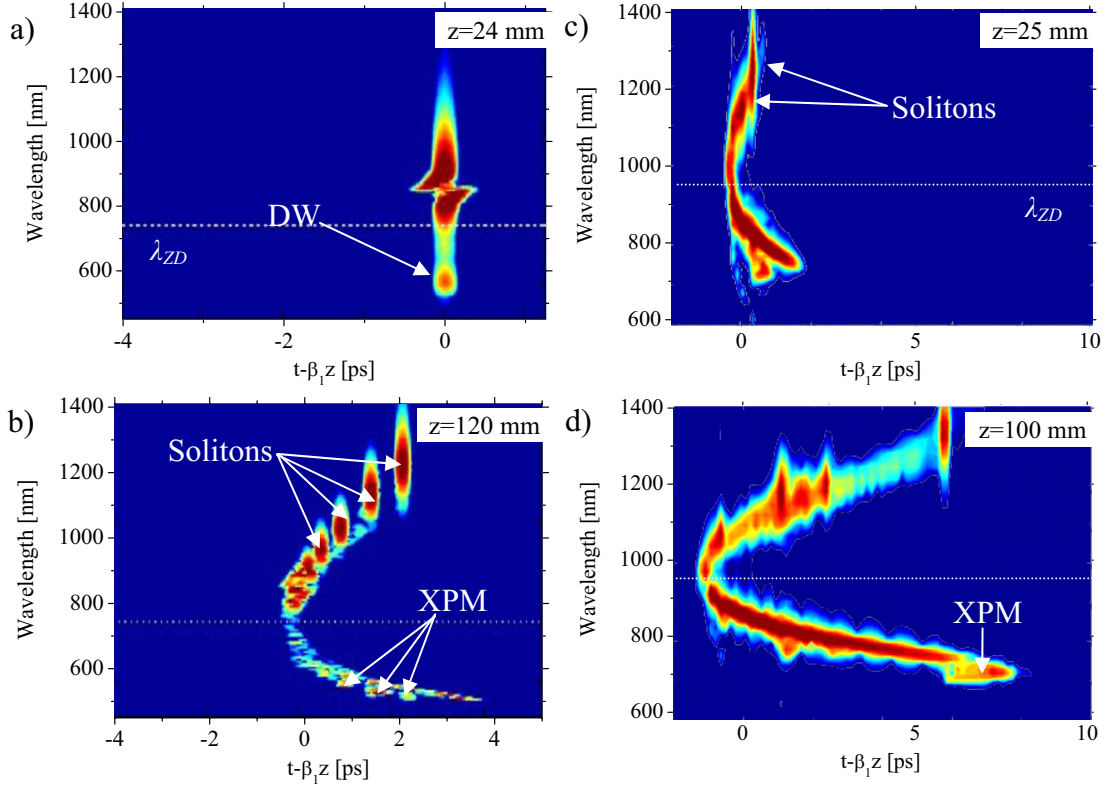


**Figure 3-2.** Calculated spectrograms of SC generation with a,b) anomalous and c,d) normal dispersion at the pump wavelength (reproduced from [P1] and Ref. [13]). The red color indicates maximum intensity and deep-blue color is 30 dB below maximum.

The spectrum of the supercontinuum can be tailored by changing the pump pulse parameters, such as pump wavelength  $\lambda_p$ , peak power  $P_p$  and pump-pulse duration  $T_{FWHM}$  [13,101]. The further  $\lambda_p$  is tuned from  $\lambda_{ZD}$ , the further to the blue the DWs will be formed as the resonant wavelength is changed. This commonly results in a gap in the spectrum located around  $\lambda_{ZD}$  [P3]. Moreover, for a longer  $\lambda_p$ , SSFS shifts the solitons further into the infrared, the exact magnitude of the shift strongly depending on the dispersion and loss profiles of the fiber. The soliton order  $N$  varies with  $\sim\sqrt{P_p}$ , and, therefore, increase of the pump power results in higher number of generated solitons. A higher number of the solitons is also increasing the amount of DWs. For a fixed value of average input power (and consequently, fixed pulse energy), varying  $T_{FWHM}$  changes  $P_p$ , thus affecting strongly the  $N$  value. Short ( $\sim 10$ -30 fs) pump pulses

result in a small number of solitons widely separated in the spectrum, and longer pump pulses ( $\sim 100$  fs) generate a smoother spectrum with reduced bandwidth.

When the wavelength of the pump pulse resides in the normal dispersion region of the fiber as in Fig 3-1b ( $\lambda_p=831$  nm,  $\lambda_{ZD}\approx 940$  nm,  $P_{av}=120$  mW,  $T_{FWHM}=130$  fs), the initial broadening is caused by SPM [13]. The magnitude of the SPM-induced broadening is mainly determined by  $P_p$ . If the spectrum extends over  $\lambda_{ZD}$  into the anomalous dispersion region, this part of the pulse reshapes into multiple fundamental solitons (Fig. 3-2c,d) which subsequently experience the SSFS.

#### *Supercontinuum generation with pico and nanosecond pump pulses*

Cost-efficient and compact pico and nanosecond pulse lasers provide few kilohertz pulse trains with peak power in the kW range which may readily be applied for supercontinuum generation [15,16,84]. A typical example is a Q-switched Nd:YAG laser, which provides hundreds of milliwatts of average power [25]. When pumping with picosecond pulses, supercontinuum generation is mostly based on FWM [15]. Stimulated Raman scattering subsequently amplifies the long-wavelength side of the spectrum. When  $\lambda_p$  is on the anomalous dispersion side and pump pulse duration is in the nanosecond regime the main broadening mechanisms are FWM followed by Raman scattering [25]. FWM breaks the pulse into multiple solitons, each of which subsequently experiences SSFS.

### **3.3 Enhancement of supercontinuum bandwidth**

The supercontinuum spectrum can be tailored by changing the MF parameters. With specially designed fibers, the SC bandwidth may be extended through, e.g., cross-phase modulation or infrared zero-dispersion wavelength. Furthermore, a highly-birefringent MF has two optical axes with different dispersion properties. These enhancements are discussed in the following paragraphs.

#### *Influence of cross-phase modulation*

In the final stages of SC generation with femtosecond pump pulses and anomalous dispersion at the pump wavelength, the SSFS shifts the solitons to longer wavelengths reducing the GV of the solitons to be slower than that of the DWs. Therefore, the DWs catch up with the solitons, allowing for interaction through XPM [P1] (Fig. 3-2b). Due to the sign of the GV mismatch between solitons and DWs, the dominant broadening induced by the soliton on the DW spectral components occurs towards the blue wavelengths extending the supercontinuum bandwidth [P1]. Note that the peak power of the solitons exceeds by far that of the DW. Consequently, the XPM broadening is mainly induced by the solitons onto the DWs and not vice versa.

Similar behavior is observed in the case of normal dispersion pumping. Again, the solitons are delayed with respect to the part of the pulse spectrum which lies in the

normal dispersion region, inducing XPM broadening of the spectrum towards shorter wavelengths (Fig. 3-2d).

#### *Enhanced bandwidth due to infrared zero-dispersion wavelength*

In most experiments performed with  $\lambda_P$  around 800 nm, the longest wavelengths obtained on the infrared side of the supercontinuum have been limited to around 1500 nm due to the strong OH-absorption at 1400 nm. This absorption reduces the energy of the solitons (thus increasing their temporal width) and thereby limiting the SSFS. Several approaches have been undertaken to extend the SC to longer wavelengths. For instance, tuning  $\lambda_P$  to longer wavelengths [13] or using a fiber made of highly nonlinear glass [42] may provide hundreds of nanometers of more bandwidth.

By reducing the core-size of MFs the second  $\lambda_{ZD}$  is pushed to shorter wavelengths at around 1500 nm. When the wavelength of the solitons is shifted into the vicinity of the second  $\lambda_{ZD}$  by SSFS, the spectrum of the solitons may overlap with that of the dispersive waves on the long-wavelength side of the infrared  $\lambda_{ZD}$  given by Eq. (3.10). Energy is then shed by the solitons to the dispersive waves, extending the spectrum to longer-wavelengths [P2]. This is clearly seen also in the experimental results shown in Fig. 3-3, obtained when pumping a MF with  $\lambda_{ZD}$  at 690 and 1390 nm. The average input power for the train of 27 fs pulses at  $\lambda_P=790$  nm was 118 mW.

Recently it was suggested by Hilligsøe *et al.* in [102], that this mechanism is different if the two  $\lambda_{ZD}$ s are spaced by only a few hundred nm. Their analysis, based on the continuous-wave theory of FWM, suggests, that in this case SPM and FWM are the causes for formation of two sidebands located symmetrically with respect to the  $\lambda_{ZD}$ .

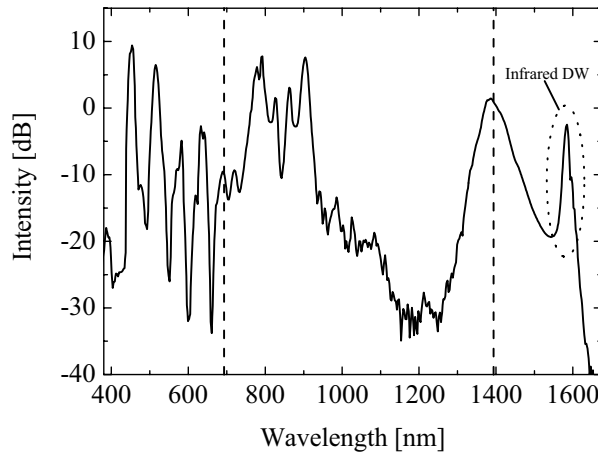


**Figure 3-3.** Supercontinuum generated in a MF with a second  $\lambda_{ZD}$  in the infrared. The dashed vertical lines mark the  $\lambda_{ZD}$ s.

#### *Highly-birefringent microstructured fiber*

Controlling the input polarization is of great importance in SC generation when using a fiber with a highly-birefringent core [P3]. In such a fiber, the polarization state of the input light can be decomposed onto the principal axes of the fiber. Due to the high

GD difference between the two axes (birefringence), both modes propagate without mutual interaction after only a few mm of propagation so that the continuum at the fiber output is essentially the linear superposition of the individual SC generated along each axis. Since the two axes exhibit different dispersion characteristics, they also allow generation of SC with different spectral features by simply tuning the polarization of the input light. For example, the phase-matching condition for the DW generation is different for the two axes (and thus the spectral features of the SC may be varied by changing the input polarization). Figure 3-4 shows SC spectra measured for different linear input polarizations for input pulse powers corresponding to  $N \approx 1.5$  (for the dispersion value of the fast axis) and anomalous dispersion at  $\lambda_P$ . The zero-dispersion wavelengths  $\lambda_{ZD}$  of this fiber (fiber core dimensions  $1.5 \times 2.3 \mu\text{m}^2$ ) are located at 635 and 700 nm for the fast and slow axis, respectively. Therefore, when the pump pulse polarization is rotated from the fast towards the slow axis, the soliton formed on the fast axis (marked with F in the figure) experiences reduced SSFS since a greater fraction of the power is coupled to the slow axis. Also, pump pulse power that excited a fundamental soliton for the dispersion value of the fast axis at  $\lambda_P$  is sufficient to excite a second-order soliton for the slow axis dispersion, which has a lower value.

Furthermore, the phase-matching condition for DW generation is different for the two axes. The overlap of the soliton with the dispersive waves is larger on the slow axis than on the fast axis where  $\lambda_{ZD}$  is 60 nm more detuned from the  $\lambda_P$ . Therefore, the intensity of the generated DW is much higher when the pump pulse polarization is aligned with the slow axis. Finally, by aligning the input polarization along one of the two axes, it is possible to have all of the input light contributing to the SC, thus maximizing the SC bandwidth [P3]. After publication of [P3], similar results have been reported by, e.g., Proulx *et al.* in [103].

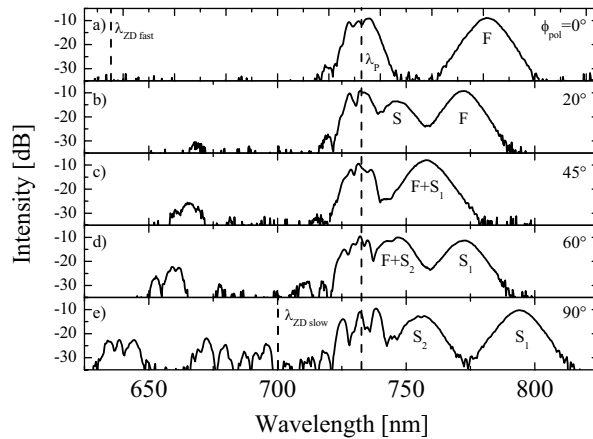


**Figure 3-4.** Experimental spectra showing the effect of input polarization on SC generation.  $\phi_{\text{pol}}$  is the angle of the input polarization with respect to the fast axis of the fiber. F=soliton propagating along the fast axis,  $S_1$ =first soliton split from the input pulse propagating on the slow axis,  $S_2$ =second soliton on the slow axis.

### 3.4 Broadband blue light generation

Ultraviolet and deep blue light is widely used in several applications ranging from spectroscopy to biomedical analysis. The availability of broad light sources for this wavelength region is very limited, and most compact sources consist of an LED or a diode laser emitting in the red with light frequency doubled to the blue. Since the introduction of broadband SC generated in MFs, there has been keen interest to extend the spectrum further into the blue wavelength region. Using only one pump pulse from, e.g., a Ti:Sapphire laser, relatively high input power is required in order to generate light below 500 nm. Moreover, in SC generation the highest fraction of the input power is transferred to infrared wavelengths. In [P4], improvement of the efficiency of blue light conversion using a two-pump scheme is proposed, and the prerequisites of the technique are presented below.

#### *Dual pumping and cross-phase modulation*

In Chapter 3.3 and in [P1] XPM was shown to enhance the bandwidth of the SC towards blue due to the group-delay difference of the frequency shifted solitons and the blue DWs. Similar effect should also occur if, e.g., a pulse and its second harmonic obtained from a mode-locked Ti:Sapphire laser as proposed in [P4] or from a compact diode-pumped Nd:YAG laser are coupled into the fiber. Here, these pulses are referred to as the pump (soliton) and the probe (second harmonic) pulse. The proposed setup for generating the pulses and to tune their relative initial delay is shown in Fig. 3-5a.

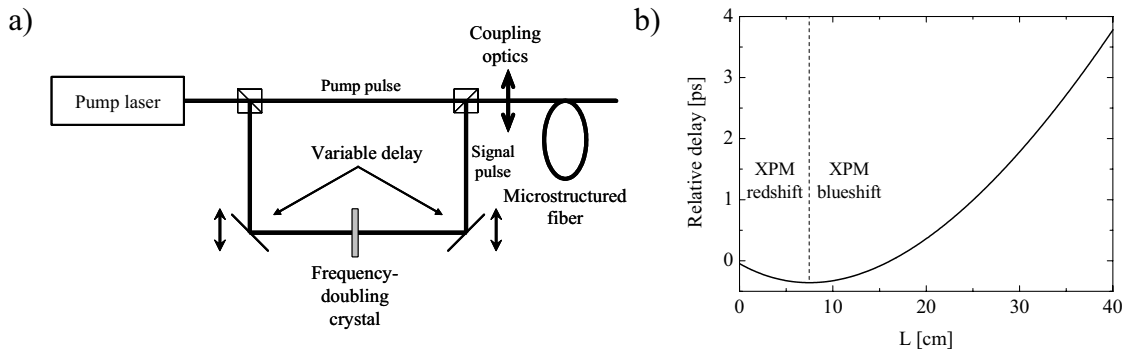


**Figure 3-5. a) Proposed experimental setup for efficient generation of broadband blue light. b) Calculated relative delay of pump and signal pulses for different values of fiber length  $L$ . A positive value of the delay stands for signal trailing the pump.**

Efficient broadening of the second-harmonic pulse requires the GD-difference of the pulses to vary [86]. This can be realized experimentally if the pump pulse corresponds to a soliton and experiences the SSFS. This condition sets the lower limit for  $P_P$  and  $T_{FWHM}$  of the input pulse, i.e., the pump pulse has to fulfill  $N \geq 0.5$ . In order to obtain efficient broadening of the probe spectrum to both red and blue directions from its center wavelength, the dispersion profile of the MF should be such that the soliton

first accelerates compared to the probe (inducing redshift), and subsequently decelerates due to SSFS (inducing blueshift) as shown in Fig 3-5b. In practice, even a nanosecond pulse can form multiple solitons due to modulation instability if the pump pulse spectrum lies in the anomalous dispersion region of the fiber, and they may thus be also applied for efficient blue-light generation [24,104].

The initial delay between the pump and probe pulses has significant effect on the induced frequency shift. If the two pulses do not entirely pass through each other along the propagation inside the MF, the XPM-induced chirp induced by the leading/trailing edge of the pump pulse onto the trailing/leading edge of the probe pulse is only partly compensated for. Therefore, by proper selection of the input delay and fiber length, one may induce mainly red, blue, or symmetrical broadening.

## 4 Spectral characterization of optical components

Transmission and absorption are fundamental properties of optical components requiring accurate characterization as they may substantially affect the performance of the setup in which the components are utilized. Several techniques have been developed for the characterization of the transmission/absorption properties of fiber-optic components [105]. Light sources widely applied for transmission or absorption measurements include light bulbs, laser diodes, LEDs and tunable lasers depending on the measurement wavelength range desired. For instance, Xenon and Tungsten-Halogen lamps are commonly employed as broad-band sources for measuring the attenuation spectrum of optical fibers as well as the absorption spectra of doped fibers. However, the incoherence of the source drastically limits the dynamic range of the measurements due to the poor coupling to the fiber. In contrast, laser diodes or tunable lasers exhibit higher spectral density and better coupling efficiency to fibers but suffer from a narrow bandwidth or limited wavelength tuning range. Therefore, the characterization might prove to be difficult in the case of high absorption or low transmission values and if a large measurement wavelength range is needed. Supercontinuum, as white laser light, combines the ease of collimation and focusing of lasers with the broad bandwidth of LEDs and light bulbs. Moreover, SC may be generated in a polarization-maintaining MF [P3], therefore allowing for the study of polarization effects in components. Some key parameters of typical broadband sources are summarized in Table 3.

In Paper [P4] SC radiation generated using two different pump lasers was applied to characterize the absorption or transmission of three novel fiber-optic components. The supercontinuum radiation was butt-coupled into the device under test with a coupling efficiency of ca. 50%. The output spectrum was recorded with an optical spectrum analyzer and was compared to the input SC in order to obtain the transmission/absorption spectrum of the component.

**Table 3. Comparison of broadband sources.**

Source	Bandwidth	Spectral density	Focusing	Polarization
<b>Light bulb</b>	visible and IR	low	very poor	unpolarized
<b>Broadband LED</b>	~100 nm	medium	poor	unpolarized
<b>Tunable laser</b>	~200 nm (tuning range)	monochromatic	excellent	linear
<b>Supercontinuum</b>	400-1600 nm	high	excellent	linear

### *Erbium-doped fibers*

Erbium-doped fibers are manufactured similarly to single-mode fibers by doping the core of an otherwise pure-silica fiber with impurity atoms. In these fibers, the dopants are  $\text{Er}^{3+}$  ions, often accompanied by co-dopants to reduce the inevitable clustering of the ions [106]. Erbium-doped fibers are the basic medium of amplifiers in optical

telecommunications since  $\text{Er}^{3+}$  provides conveniently gain at around 1530 nm when pumped at 980 nm or 1480 nm. The length of fiber needed to obtain a fixed value of gain is determined by the amount of absorption at these wavelengths. The absorption of modern high-concentration doped fibers is far too high to be measured using a conventional broadband source for reasonable lengths of fiber. However, using SC radiation the transmission spectrum of two high concentration Erbium-doped fibers could easily be obtained over a broad range [P5].

The absorption spectrum of  $\text{Er}^{3+}$  consists of several lines, corresponding to one transition from the ground state  $^4\text{I}_{15/2}$  to higher energy states [106]. The relevant energy level structure of  $\text{Er}^{3+}$  in a solid host is shown in Fig. 4-1.

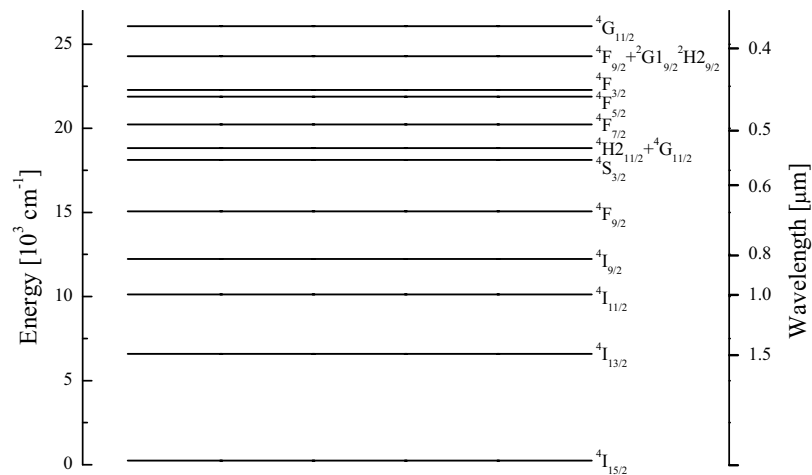


**Figure 4-1. Energy level structure of  $\text{Er}^{3+}$ .**

In addition to transitions involving absorption of a single photon from the light field, processes where an ion in an excited state is further transferred to a higher energy excited state by absorbing a second photon are also possible. Such step-wise two-photon transitions are difficult to study, since a large number of pump photons is required at exotic wavelengths, for which it is difficult to find a laser source. Here SC turns out to be very useful, since by coupling the SC light into the fiber, all the absorption transitions are excited simultaneously. In [P5] it was found that this is indeed the case when a ns pulse pumped SC source is used, as the high energy of the ns SC pulses was sufficient to allow many new excited-state absorption transitions. In particular, strong absorption was observed at 709 nm and 845 nm and a weak blue emission peak located at around 480 nm, as shown in Fig. 4-2 for a highly-doped fiber sample. Also, it was noticed that the relative magnitude of these peaks was strongly intensity-dependent, which is typical for two-photon absorption. Indeed, the energy difference between the  $^4\text{I}_{13/2}$  and  $^4\text{F}_{7/2}$  levels of  $\text{Er}^{3+}$  corresponds to around 710 nm and the energy difference between the  $^4\text{F}_{7/2}$  level and the ground state is nearly equal to 480 nm. The peak at around 845 nm as well as the peak at 790 nm correspond to absorption from an excited state of  $\text{Er}^{3+}$  ( $^4\text{I}_{13/2} \rightarrow ^2\text{H}_{11/2}$  and  $^4\text{I}_{13/2} \rightarrow ^4\text{S}_{3/2}$ , respectively).

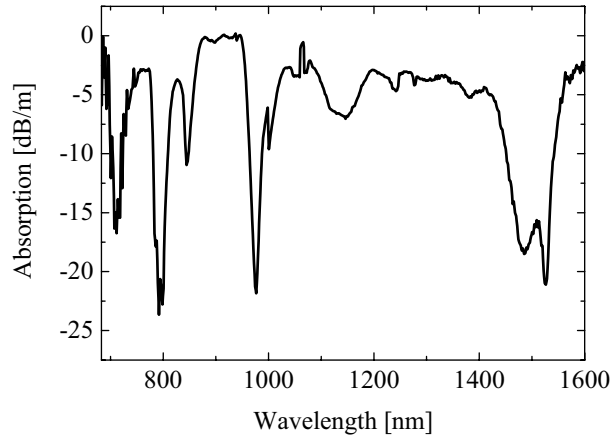


**Figure 4-2. Absorption spectrum of a highly-doped fiber sample measured using a nanosecond supercontinuum as the light source.**

*Transmission spectrum of photonic bandgap fibers*

The characterization of the transmission spectrum of photonic bandgap fibers is hindered by the incoherence of lamps commonly employed as broadband sources for these studies. In [P5], supercontinuum light allowed not only to characterize the transmission band of the fiber, but also to study light coupling to short-wavelength cladding modes by careful control of the input misalignment [107]. In Fig. 4-3, the transmission spectrum of a 5 m piece of PBF measured by using supercontinuum illumination is shown when the input beam is misaligned. Accurate characterization of these effects is required in order to further optimize the design of low-loss bandgap fibers.

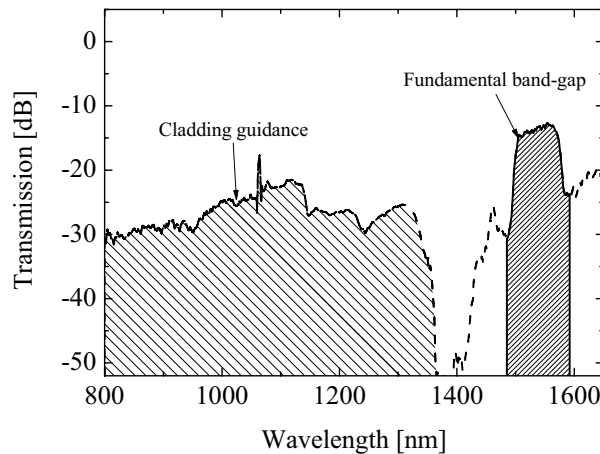


**Figure 4-3. Measured fundamental bandgap and cladding guidance in PBFs.**

*High-finesse fiber cavity*

High-finesse fiber-cavities can be realized by depositing several thin-film layers onto the fiber connectors which then form high-reflectivity mirrors. High-finesse fiber cavities have attractive possibilities. For instance, if the core of the fiber is exposed from the middle of the cavity by etching or by tapering, the long ring-down time

allows for efficient evanescent-wave sensing [108]. Moreover, high power oscillating inside the cavity opens up possibilities for several nonlinear applications, such as switching by optical bistability. However, characterization of the broadband mirrors employed in high-finesse fiber cavities is difficult using incoherent sources such as light bulbs. Supercontinuum light can easily be coupled through the fiber cavity, directly giving access to the transmission spectrum of the component [P5].

Transmission spectrum of a fiber cavity is determined by the Airy-function as

$$I_T(\lambda) = \frac{I}{1 + \frac{4F(\lambda)^2}{\pi^2} \sin^2(\beta(\lambda)L)} I_0, \quad (4.1)$$

where  $\beta$  is the propagation constant of the fiber,  $L$  is the cavity length, and  $F$  is the cavity finesse given by

$$F = \frac{\Delta f}{\delta f_{1/2}} = \frac{\pi\sqrt{R}}{1-R}, \quad (4.2)$$

where  $\Delta f = c/2nL$  is the frequency spacing between two consecutive transmission maxima and  $\delta f_{1/2} = (1-R)c/2\pi nLR^{1/2}$  is the full-width at half maximum of the transmission peak.  $R$  is the mirror reflectivity. Total power transmitted through one period of the transmission spectrum of a high-finesse cavity is then  $P_{out} = P_{in}(1-R)/4R^{1/2} = \pi P_{in}/4F$ . If the cavity is illuminated using a broadband source (such as SC), and the spectrum is measured using a device which measures the power with resolution much broader than the FSR (such as an optical spectrum analyzer), the average power measured for each sample is then also obtained from the same equation. In [P5], we used this relation to characterize the reflectivity of the cavity mirrors using a SC as the light source.

## 5 Optical components based on microstructured fibers

Microstructured fibers have opened up the road for numerous applications and components. In this Chapter, application of tapered MFs for coupling to photonic crystal waveguides and a MF based all-optical switch are discussed.

### 5.1 Tapered microstructured fibers for coupling to photonic crystals

Photonic crystals (PCs) allow for novel ways to manipulate the flow of light and have shown great potential for many applications in the field of optics. These include low-loss waveguides with sharp bends, omnidirectional mirrors, inhibition of spontaneous emission, and various passive/active optical functions [35]. For practical handling considerations, PCs are typically manufactured on chips of larger dimensions and waveguides are channeled from the edges of the chip to allow coupling of light into the PC. A major issue is then the efficiency of the coupling. Preferably the light should be launched into the waveguide by using a fiber-based coupling setup. The PC waveguides are usually very thin, on the order of hundreds of nanometers, in order to ensure pure transverse photonic bandgap guidance along the PC region. This severely limits the coupling efficiency of light from SMFs since the dimensions of the SMF output mode and the waveguide input mode are quite different.

#### *Coupling techniques*

The simplest way of coupling light from a standard fiber into a PC waveguide consists of focusing a free-space beam with a lens or using a specially tailored fiber spliced to the end of the standard fiber [57]. Tailored waveguides may also be used as a mode-converter. The fiber-end of such a waveguide is of larger dimensions for better coupling efficiency from fiber to waveguide, and the width of the other end of the waveguide is reduced to the dimensions of the defect of the PC [109,110]. A similar structure can also be used in the output end of the PC to provide good extraction efficiency. It has also been demonstrated that it is possible to taper the height of the input waveguide [111]. The resulting input facet of the waveguide is square, providing large overlap with the fundamental mode of a standard optical fiber, thus reducing the coupling losses. Increasing the input mode-field diameter of the PC may also be achieved by tapering the width of the PC waveguide so that it is larger closer to the input [112,113]. The manufacturing is, however, difficult since the waveguiding parameters of the PC change as more holes are removed or shifted to form a larger defect. Such a technique would thus require a rather complex analysis.

The large difference between the areas of the fiber core and the fundamental mode propagating in the waveguide results in a poor mode-overlap. The overlap can be improved if a taper is used as an adapter between the SMF and the PC waveguide. The diameter of a tapered fiber is gradually reduced, so that the MFD of the propagating mode adiabatically reduces [114]. This can be realized, e.g., by

simultaneously heating the fiber with a flame or a high-power laser and elongating it [115]. It is possible to manufacture a taper spliced from the input end to a SMF with negligible losses, and of which the diameter in the output end has been reduced to the dimensions of the PC waveguide [36,116,117]. In practice, the MFD of a tapered fiber can be decreased down to 200 nm although diameters below 1  $\mu\text{m}$  require more complex techniques than the standard laser or flame heating and pulling [118]. A major problem with small-diameter tapered SMF is the fact that the taper mode is only confined by the silica-air interface. This makes the handling of tapered standard fibers difficult, since any physical contact or obstacle in the vicinity of the tapered section disturbs the propagating field, thus increasing the losses. Tapers have been used in experiments and several studies have been conducted in order to minimize the transition length of the taper, making the component more robust and rigid (see, e.g., [119,120]). Another problem associated with tapers with extremely small dimensions is that the more the diameter is reduced, the more fragile the taper becomes. This is a known consequence of the increasing number of heat/melt/cool cycles in the tapering process, which eventually leads to crystallization of the silica [121,122].

Reducing the diameter of a standard fiber to the order of a few micrometers results in a transition of the guided mode from the core-cladding interface to the silica-air interface [60]. Most of the field energy then propagates in the evanescent field which decays exponentially in the air surrounding the taper. Several applications have been developed for such tapered fibers, e.g., fiber couplers and coupling to whispering-gallery resonators [123,124]. The evanescent field of a tapered standard fiber has recently been applied for coupling light from a fiber to a PC-waveguide. In such a coupling system, the tapered fiber is positioned a few micrometers above the waveguide so that the evanescent fields of the propagating mode of the taper and that of the PC are in resonance. The theoretical limit for the coupling efficiency is 100%, and recently a coupling efficiency of 94% was obtained experimentally [125-127].

#### *Tapered microstructured fiber*

Fiber tapering provides a convenient way to reduce the mode-field diameter (MFD) of fibers and may therefore allow for a better coupling efficiency to a PC waveguide [36,37]. In the case of tapered SMFs, light leaks out of the core of the fiber and is guided inside the whole cladding due to the refractive index difference between silica and the surrounding air [119]. Consequently, in order to obtain a small MFD in the output, a large reduction factor of the initial outer diameter of the fiber is required resulting in a structure that is fragile and difficult to handle. This can be improved by tapering a MF [128,129]. The main advantage of MFs over SMFs lies in the fact that the microstructure of MFs is preserved during the tapering process and, therefore, light remains guided inside the core [129]. This difference between tapered SMFs and MFs is crucial as the MFD at the output of the tapered MF scales as the reduction of the initial core diameter. Therefore, the diameter of the fiber needs to be decreased by only a factor of 10 of the original diameter to obtain a MFD as small as 1  $\mu\text{m}$  compared to a factor of 100 in the case of a SMF. Robustness of the taper is

consequently greatly improved and handling is expected to be much easier. Moreover, another direct consequence lies in the possibility of reducing substantially the length of the transition region of tapered MFs compared to tapered SMFs [128]. The MFD can be adiabatically reduced along a tapered MF provided the taper profile is properly designed [119,130]. An important benefit of tapered MFs compared to SMF is, that the output mode-field can be made asymmetric by simply tailoring the microstructured cladding of the fiber.

#### *Setup for coupling to photonic crystal waveguide*

Paper [P6] deals with the possibility of employing a tapered MF for efficient light coupling from a standard SMF to the rectangular input of a waveguide of dimensions  $5 \mu\text{m} \times 200 \text{ nm}$  used as a channel for a PC. The coupling setup is depicted in Fig. 5-1. A SMF is directly spliced to the input of a tapered MF in front of the input waveguide of the PC. The PC into which coupling is studied consists of a silicon-on-insulator chip with an etched triangular array of air-holes (pitch  $A_{PC}=2 \mu\text{m}$ , hole diameter  $d_{PC}=0.8 \mu\text{m}$ ). Light is confined in the vertical direction by the insulator layer and air. The guiding layer is 200 nm thick, resulting in a strong ellipticity of the propagating modes ( $e > 99\%$ ). The width and height of the input ridge waveguides are  $w=5 \mu\text{m}$  and  $d=200 \text{ nm}$ , respectively.

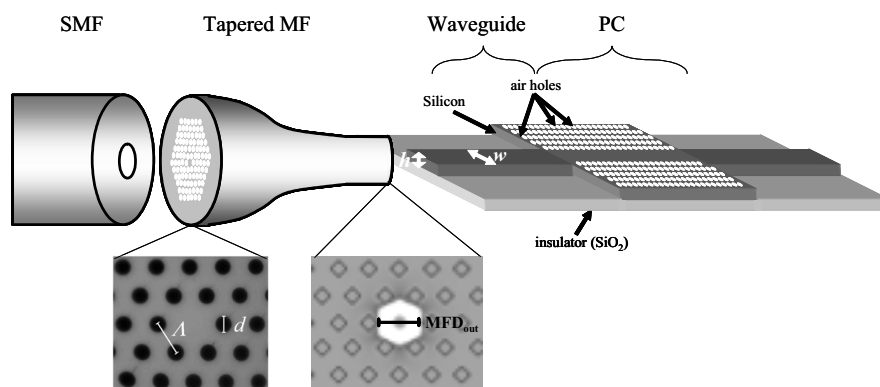


**Figure 5-1. Tapered microstructured fiber for coupling between SMF and PC waveguide.**

The coupling efficiency to the waveguide is increased for smaller values of output mode-field diameter  $MFD_{out}$  as seen in the simulation results obtained using the beam-propagation method (see Fig. 5-2a). However, due to its large width the waveguide is highly multimode and part of the energy propagates in higher-order modes. Coupling light mainly to the fundamental mode of the waveguide is essential due to the modal behavior of the PC. Indeed, the coupling efficiency from the input waveguide to the PC itself is optimal only when light propagates in the fundamental mode of the input waveguide. If various modes are excited in the waveguide, the mode-field distribution of the output of the waveguide may be complex and propagation inside the PC severely perturbed. The distribution of power to different modes is shown in Fig. 5-2b for some of the TE-modes that can propagate in the waveguide. The fundamental mode will be solely excited only if the dimensions of

$MFD_{out}$  and that of the waveguide are on the same order (see Fig. 5-2b), which is not the case for small  $MFD_{out}$  values.

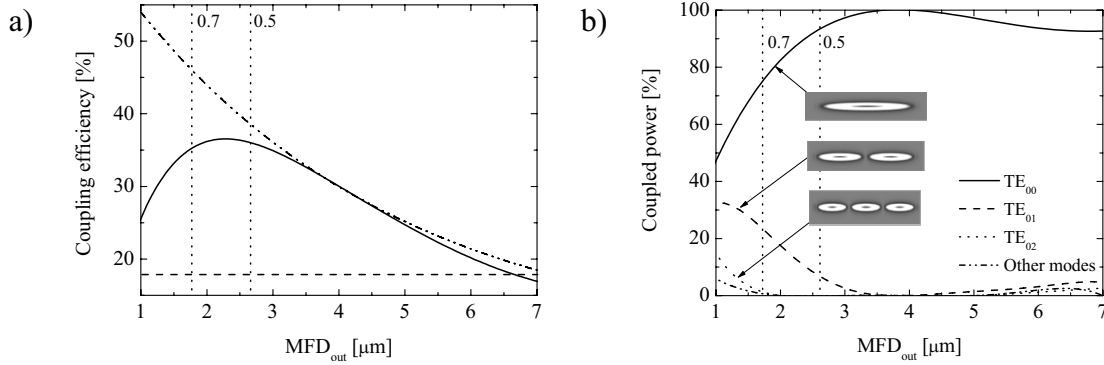


**Figure 5-2.** a) Simulated coupling efficiency to the waveguide including all losses (dashed-dotted line) and coupling efficiency to the fundamental mode of the waveguide (solid line). The dashed horizontal line shows the coupling efficiency obtained using SMF. b) Simulated distribution of the coupled power over different modes of the waveguide. In both figures the dotted vertical lines show the minimum attainable  $MFD_{out}$  for MFs with  $d/\Lambda$  of 0.5 and 0.7.

The main limitation to the coupling efficiency originates from the mismatch between the vertical dimensions of the  $TE_{00}$  modes of the waveguide and the tapered MF. This mismatch may be reduced by tapering an elliptic-core MF, e.g., a highly birefringent MFs [5]. Even though this will also increase the splice loss with the SMF at the input of the tapered MF, matching the smaller dimension of the core of the MF with the core diameter of the SMF should, however, result only in a slight increase of the loss. Another advantage of the elliptical-core MFs lies in the preservation of the polarization [131], which may be crucial for proper functioning of the PC as it is extremely sensitive to the input polarization.

## 5.2 Microstructured fiber based switch

Nonlinear fiber cavities, formed by a piece of fiber with mirrors in both ends or by forming a fiber loop using couplers, can lead to several interesting phenomena such as optical bistability, self pulsing, period doubling, power limiting, and chaos [132]. Some of these may find applications in optical communications. For example, switching [38] and flip-flop operation in standard fiber based cavities have been demonstrated [39].

### *Optical bistability in nonlinear cavities*

The transmission spectrum of a nonlinear fiber cavity is determined by the cavity length, dispersion of the fiber and optical power oscillating in the cavity. For continuous wave input signals, maximal transmission is obtained when the frequency of the signal is offset by a frequency difference which compensates for the nonlinear phase-shift  $\phi_{NL}$  induced by the power oscillating in the cavity (see Fig. 5-3)

$$\phi_{NL}^{SPM} = \gamma P, \quad (5.1)$$

where the nonlinear coefficient  $\gamma$  is given by

$$\gamma = \frac{n_2 \omega}{c A_{eff}}. \quad (5.2)$$

Here  $n_2$  is the nonlinear refractive index of silica,  $\omega$  marks the angular frequency,  $c$  denotes the speed of light, and  $A_{eff}$  is the effective area of the propagating mode. The dependence of the transmission function of the cavity on input power results in bistable behavior [133]. The exact shape of the transmission function is not solely determined by the cavity length and nonlinearity, but also by the cavity loss. Efficient operation of any bistable component requires either minimization of losses in the cavity, or addition of an amplifier inside the cavity. Bistability is, indeed, often observed in high-power lasers such as, e.g., CO<sub>2</sub> lasers [134]. When the input power of a bistable cavity is increased beyond the value corresponding to the maximum transmission level, the transmission function becomes very unstable, which is often referred to as optical chaos or Ikeda instability.

There are two main types of fiber cavities. The first type is typically constructed from a piece of fiber and one or two fiber couplers forming a fiber loop. An optical isolator is usually placed in the cavity in order to ensure unidirectional propagation. Furthermore, the isolator also suppresses stimulated Brillouin scattering, which otherwise would limit the efficiency of the device. The second type is based on forming two mirrors in both ends of a short piece of fiber. Current manufacturing technologies allow to deposit dielectric mirrors with reflectivities higher than 0.99 at the end facets of standard fiber connectors. Both cavity types exhibit bistable behavior at high input powers. The analysis of the latter type is, however, somewhat more complex, since the counter propagating beams must be included.

Optical bistability using continuous-wave signals has only a small number of applications. With pulsed input, the hysteresis of the cavity can, e.g., be used for pulse compression or optical switching. In this case, the behavior depends on the relative magnitudes of the cavity round-trip time  $\tau_{cav}$  and the bit rate/pulse duration. If  $\tau_{cav}$  equals the bit rate of the input signal, only the part of the pulse exceeding the bistable switching threshold power is amplified, which reduces the pulse duration. If the input pulse duration is significantly longer than  $\tau_{cav}$ , then the shape of the transmitted pulse may be very complex and requires the use of numerical analysis.

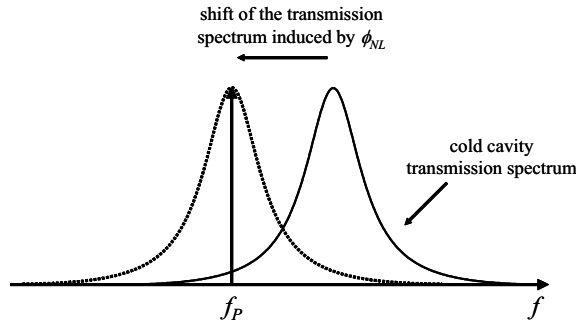


**Figure 5-3** Effect of nonlinearity on the transmission spectrum of a high-finesse fiber cavity.  $f_P$  denotes the pump frequency.

### *All-optical flip-flop*

In paper [P7] a highly nonlinear MF based bistable cavity in a loop configuration with two couplers is proposed. The loop configuration was chosen due to the simplicity of the analysis, i.e., only unidirectional propagation needed to be considered if an isolator is inserted in the cavity. The application of the cavity as an all-optical flip-flop was numerically simulated. The switch operates with a continuous wave bias with frequency slightly detuned from the maximum of the transmission spectrum, and switches signal from the input to one of the two outputs of the loop cavity. The active output is selected by introducing either a high or a low pulse to the bias signal. Similar components have previously been demonstrated using standard fibers. However, their efficiency has been significantly limited due to the required long fiber length or high pump powers. High nonlinearity of MFs suppresses these limitations, making nonlinear MF based cavities very attractive components for optical signal processing.

## 6 Summary

This dissertation presents several novel applications of microstructured fibers developed within the Fiber-Optics Group of Helsinki University of Technology during the years 2002-2005. The first half of the thesis is dedicated to broadband light sources based on microstructured fibers. In [P1], soliton-induced cross-phase modulation was identified as the effect responsible for creating new frequency components in the final stages of supercontinuum generation. Furthermore, two tailored fiber designs were studied within this work. In particular, a second zero-dispersion wavelength in the infrared region was found to extend the supercontinuum spectrum due to leakage of dispersive radiation from a frequency-shifted soliton to a resonant wavelength. This reduces the required pump power for efficient continuum generation [P2]. Moreover, use of a highly-birefringent polarization maintaining fiber in supercontinuum generation allows for tuning of the spectral characteristics of the continuum by choosing the distribution of the input power along the principal polarization axes of the fiber [P3]. In [P4], generation of broadband radiation covering more than 1000 nm is predicted when pumping a microstructured fiber with a tailored dispersion profile using two pump pulses. The pump power required for the process is 20 dB less than in supercontinuum generation, thus allowing for the development of miniaturized coherent broadband sources. Since the appearance of [P4], Konorov *et al.* have published experimental results [135], which are in good agreement with the predictions.

The second half of the work considers new applications for microstructured fibers and supercontinuum light. In [P5], supercontinuum radiation generated in microstructured fibers is applied to characterization of the transmission or absorption of various optical components. In particular, nanosecond-pulse pumped supercontinuum permitted for observing several excited-state absorption transitions of  $\text{Er}^{3+}$ , which were otherwise unavailable due to lack of sources at these wavelengths. The intense supercontinuum spectrum was also found to be valuable when studying the transmission spectrum of a photonic bandgap fiber and a high-finesse fiber cavity. Both of these components have strong variations in their transmission spectrum immeasurable using conventional white-light sources.

The possibility of employing a tapered microstructured fiber for efficient light coupling from a standard SMF to the rectangular input of a waveguide of dimensions  $5 \mu\text{m} \times 200 \text{nm}$  was investigated in [P6]. Such waveguide is used for example as a channel to couple efficiently to photonic crystals. Numerical simulations were performed using beam-propagation method to design the profile of the taper in order to minimize the losses along the taper transition. Using the same method, the coupling efficiency to the waveguide was subsequently simulated and the relative distribution of the power coupled into different modes of the waveguide was studied. An optimum diameter was found for the core of the tapered MF to maximize the coupling

efficiency to the fundamental mode of the waveguide. In order to further increase the coupling efficiency limited by the small vertical dimension of the waveguide, a tapered MF with an elliptical core was suggested. Finally, the effect of misalignment between the tapered MF and the waveguide were investigated.

Paper [P7] considers a nonlinear microstructured fiber based loop cavity. Transmission of such a cavity is strongly intensity dependent exhibiting bistable behavior. A novel design is proposed for an all-optical microstructured fiber-based flip flop. The switching threshold of the component is significantly lower than in previously demonstrated setups due to higher nonlinearity of the microstructured fiber.

## References

- [1] P. Kaiser, E. A. J. Marcatili, and S. E. Miller, "A new optical fiber", *Bell Syst. Tech. J* **52**, 265-269 (1973).
- [2] J. C. Knight, T. A. Birks, P. St. J. Russell, and D. M. Atkin, "All-silica single-mode optical fiber with photonic crystal cladding", *Opt. Lett.* **21**, 1547-1549 (1996).
- [3] P. Russell, "Photonic crystal fibers", *Science* **299**, 358-362 (2003).
- [4] N. G. R. Broderick, T. M. Monro, P. J. Bennett, and D. J. Richardson, "Nonlinearity in holey optical fibers: measurement and future opportunities", *Opt. Lett.* **24**, 1395-1397 (1999).
- [5] A. Ortigosa-Blanch, J. C. Knight, W. J. Wadsworth, J. Arriaga, B. J. Mangan, T. A. Birks, and P. St. J. Russell, "Highly birefringent photonic crystal fibers", *Opt. Lett.* **25**, 1325-1327 (2000).
- [6] N. A. Mortensen and J. R. Folkenberg, "Low-loss criterion and effective area considerations for photonic crystal fibres", *J. Opt. A-Pure Appl. Opt.* **5**, 163-167 (2003).
- [7] J. C. Knight, T. A. Birks, R. F. Cregan, P. St. J. Russell, and J.-P. de Sandro, "Large mode area photonic crystal fiber", *Electron. Lett.* **34**, 1347-1348 (1998).
- [8] N. A. Mortensen, J. R. Folkenberg, P. M. W. Skovgaard, and J. Broeng, "Numerical aperture of single-mode photonic crystal fibers", *IEEE Photonics Technol. Lett.* **14**, 1094-1096 (2002).
- [9] A. Bjarklev, J. Broeng, and A. S. Bjarklev, *Photonic Crystal Fibres*, Kluwer Academic Publishers, London (2003).
- [10] T. Ritari, J. Tuominen, J. C. Petersen, T. Sørensen, T. P. Hansen, H. Simonsen, and H. Ludvigsen, "Gas sensing using air-guiding photonic bandgap fibers", *Opt. Express* **12**, 4080-4087 (2004).
- [11] J. K. Ranka, R. S. Windeler, and A. J. Stentz, "Visible continuum generation in air-silica microstructure optical fibers with anomalous dispersion at 800 nm", *Opt. Lett.* **25**, 25-27 (2000).
- [12] A. V. Husakou and J. Herrmann, "Supercontinuum generation of higher-order solitons by fission in photonic crystal fibers", *Phys. Rev. Lett.* **87**, 203901 (2001).
- [13] G. Genty, M. Lehtonen, H. Ludvigsen, J. Broeng, and M. Kaivola, "Spectral broadening of femtosecond pulses into continuum radiation in microstructured fibers", *Opt. Express* **10**, 1083-1098 (2002).
- [14] A. Apolonski, B. Povazay, A. Unterhuber, W. Drexler, W. J. Wadsworth, J. C. Knight, and P. St. J. Russell, "Spectral shaping of supercontinuum in a cobweb photonic-crystal fiber with sub-20-fs pulses", *J. Opt. Soc. Am. B-Opt. Phys.* **19**, 2165-2170 (2002).
- [15] S. Coen, A. H. L. Chau, R. Leonhardt, J. D. Harvey, J. C. Knight, W. J. Wadsworth, and P. St. J. Russell, "Supercontinuum generation by stimulated Raman scattering and parametric four-wave mixing in photonic crystal fibers", *J. Opt. Soc. Am. B-Opt. Phys.* **19**, 753-764 (2002).
- [16] J. M. Dudley, L. Provino, N. Grossard, H. Maillotte, R. S. Windeler, B. J. Eggleton, and S. Coen, "Supercontinuum generation in air-silica microstructured fibers with nanosecond and femtosecond pulse pumping", *J. Opt. Soc. Am. B* **19**, 765-771 (2002).
- [17] J. Herrmann, U. Griebner, N. Zhavoronkov, A. Husakou, D. Nickel, J. C. Knight, W. J. Wadsworth, P. St. J. Russell, and G. Korn, "Experimental evidence for supercontinuum generation by fission of higher-order solitons in photonic fibers", *Phys. Rev. Lett.* **88**, (2002).
- [18] A. V. Husakou and J. Herrmann, "Supercontinuum generation, four-wave mixing, and fission of higher-order solitons in photonic-crystal fibers", *J. Opt. Soc. Am. B-Opt. Phys.* **19**, 2171-2182 (2002).
- [19] A. Ortigosa-Blanch, J. C. Knight, and P. St. J. Russell, "Pulse breaking and supercontinuum generation with 200-fs pump pulses in photonic crystal fibers", *J. Opt. Soc. Am. B-Opt. Phys.* **19**, 2567-2572 (2002).
- [20] L. Tartara, I. Cristiani, V. Degiorgio, F. Carbone, D. Faccio, and M. Romagnoli, "Nonlinear propagation of ultrashort laser pulses in a microstructured fiber", *J. Nonlinear Opt. Phys. Mater.* **11**, 409-419 (2002).
- [21] B. R. Washburn, S. E. Ralph, and R. S. Windeler, "Ultrashort pulse propagation in air-silica microstructure fiber", *Opt. Express* **10**, 575-580 (2002).
- [22] W. J. Wadsworth, A. Ortigosa-Blanch, J. C. Knight, T. A. Birks, T. P. M. Man, and P. St. J. Russell, "Supercontinuum generation in photonic crystal fibers and optical fiber tapers: a novel light source", *J. Opt. Soc. Am. B-Opt. Phys.* **19**, 2148-2155 (2002).
- [23] S. C. Buchter, M. Kaivola, and H. Ludvigsen, "Compact, spectrally smooth, nanosecond infrared continuum source with 700 nm bandwidth", in *Optical Fiber Communication Conference (OFC 04)*, in Los Angeles, CA, US, 2004, paper ThA7.
- [24] S. C. Buchter, M. Kaivola, H. Ludvigsen, and K. P. Hansen, "Miniature supercontinuum laser sources", in *Conference on Lasers & Electro-Optics (CLEO'04)*, in San Francisco, CA, 2004, paper CTuP58.

- [25] W. J. Wadsworth, N. Joly, J. C. Knight, T. A. Birks, F. Biancalana, and P. St. J. Russell, "Supercontinuum and four-wave mixing with Q-switched pulses in endlessly single-mode photonic crystal fibres", *Opt. Express* **12**, 299-309 (2004).
- [26] T. A. Birks, W. J. Wadsworth, and P. St. J. Russell, "Supercontinuum generation in tapered fibers", *Opt. Lett.* **25**, 1415-1417 (2000).
- [27] S. A. Diddams, D. J. Jones, J. Ye, S. T. Cundiff, J. L. Hall, J. K. Ranka, R. S. Windeler, R. Holzwarth, T. Udem, and T. W. Hänsch, "A direct link between microwave and optical frequencies with a 300 THz femtosecond laser comb", *Phys. Rev. Lett.* **84**, 5102-5105 (2000).
- [28] A. F. Fercher, W. Drexler, C. K. Hitzenberger, and T. Lasser, "Optical coherence tomography - principles and applications", *Rep. Prog. Phys.* **66**, 239-303 (2003).
- [29] S. T. Sanders, "Wavelength-agile fiber laser using group-velocity dispersion of pulsed super-continua and application to broadband absorption spectroscopy", *Appl. Phys. B* **75**, 799-802 (2002).
- [30] C. Dunsby, P. M. P. Lanigan, J. McGinty, D. S. Elson, J. Requejo-Isidro, I. Munro, N. Galletly, F. McCann, B. Treanor, B. Önfelt, D. M. Davis, M. A. A. Neil, and P. M. W. French, "An electronically tunable ultrafast laser source applied to fluorescence imaging and fluorescence lifetime imaging microscopy", *J. Phys. D* **37**, 3296-3303 (2004).
- [31] B. Temelkuran and E. Ozbay, "Experimental demonstration of photonic crystal based waveguides", *Appl. Phys. Lett.* **74**, 486-488 (1999).
- [32] D. N. Chigrin, A. V. Lavrinenko, D. A. Yarotsky, and S. Gaponenko, "Observation of total omnidirectional reflection from a one-dimensional dielectric lattice", *Appl. Phys. A-Mater. Sci. Process.* **68**, 25-28 (1999).
- [33] J. N. Winn, Y. Fink, S. H. Fan, and J. D. Joannopoulos, "Omnidirectional reflection from a one-dimensional photonic crystal", *Opt. Lett.* **23**, 1573-1575 (1998).
- [34] E. Yablonovitch, "Inhibited spontaneous emission in solid-state physics and electronics", *Phys. Rev. Lett.* **58**, 2059-2062 (1987).
- [35] J. D. Joannopoulos, R. D. Meade, and J. N. Winn, *Photonic Crystals: Molding the Flow of Light*, Princeton University Press, New Jersey (1995).
- [36] H. Yamagawa, T. Ono, and A. Oyobe, "Mode-field-converting fiber for coupling to photonic devices", *Electron. Commun. Jpn. Pt. II-Electron.* **77**, 28-37 (1994).
- [37] K. Yoshida and T. Morikawa, "Mode-field converting fibre fabricated from a side-hole fibre", *Electron. Lett.* **32**, 758-759 (1996).
- [38] J. E. Heebner and R. W. Boyd, "Enhanced all-optical switching by use of a nonlinear fiber ring resonator", *Opt. Lett.* **24**, 847-849 (1999).
- [39] T. Fukushima and T. Sakamoto, "Kerr-effect-induced S-R flip-flop operation in an optical-fiber loop resonator with double couplers", *Opt. Lett.* **20**, 1119-1121 (1995).
- [40] J. Canning, E. Buckley, and K. Lyytikäinen, "Propagation in air by field superposition of scattered light within a Fresnel fiber", **28**, 230-232 (2003).
- [41] J. Canning, E. Buckley, K. Lyytikäinen, and T. Ryan, "Wavelength dependent leakage in a Fresnel-based air-silica structured optical fibre", *Opt. Commun.* **205**, 95-99 (2002).
- [42] V. V. Ravi Kanth Kumar, A. K. George, W. H. Reeves, J. C. Knight, and P. St. J. Russell, "Extruded soft glass photonic crystal fiber for ultrabroad supercontinuum generation", *Opt. Express* **10**, 1520-1525 (2002).
- [43] T. A. Birks, J. C. Knight, and P. St. J. Russell, "Endlessly single-mode photonic crystal fiber", *Opt. Lett.* **22**, 961-963 (1997).
- [44] R. K. Sinha and S. K. Varshney, "Dispersion properties of photonic crystal fibers", *Microw. Opt. Technol. Lett.* **37**, 129-132 (2003).
- [45] J. E. Sharping, M. Fiorentino, P. Kumar, and R. S. Windeler, "Optical parametric oscillator based on four-wave mixing in microstructure fiber", *Opt. Lett.* **27**, 1675-1677 (2002).
- [46] M. D. Nielsen, C. Jacobsen, N. A. Mortensen, J. R. Folkenberg, and H. R. Simonsen, "Low-loss photonic crystal fibers for transmission systems and their dispersion properties", *Opt. Express* **12**, 1372-1376 (2004).
- [47] T. Ritari, T. Niemi, H. Ludvigsen, M. Wegmuller, N. Gisin, J. R. Folkenberg, and A. Pettersson, "Polarization-mode dispersion of large mode-area photonic crystal fibers", *Opt. Commun.* **226**, 233-239 (2003).
- [48] J. Limpert, T. Schreiber, S. Nolte, H. Zellmer, A. Tünnermann, R. Iliew, F. Lederer, J. Broeng, G. Vienne, A. Pettersson, and C. Jakobsen, "High-power air-clad large-mode-area photonic crystal fiber laser", *Opt. Express* **11**, 818-823 (2003).
- [49] W. J. Wadsworth, R. M. Percival, G. Bouwmans, J. C. Knight, and P. St. J. Russell, "High power air-clad photonic crystal fibre laser", *Opt. Express* **11**, 48-53 (2003).

- [50] M. Moenster, P. Glas, G. Steinmeyer, and R. Iliew, "Mode-locked Nd-doped microstructured fiber laser", *Opt. Express* **12**, 4523-4528 (2004).
- [51] A. Cucinotta, F. Poli, and S. Selleri, "Design of erbium-doped triangular photonic-crystal-fiber-based amplifiers", *IEEE Photonics Technol. Lett.* **16**, 2027-2029 (2004).
- [52] G. Bouwmans, R. M. Percival, W. J. Wadsworth, J. C. Knight, and P. St. J. Russell, "High-power Er : Yb fiber laser with very high numerical aperture pump-cladding waveguide", *Appl. Phys. Lett.* **83**, 817-818 (2003).
- [53] N. A. Mortensen, M. D. Nielsen, J. R. Folkenberg, A. Pettersson, and H. R. Simonsen, "Improved large-mode-area endlessly single-mode photonic crystal fibers", *Opt. Lett.* **28**, 393-395 (2003).
- [54] J. C. Knight, J. Broeng, T. A. Birks, and P. St. J. Russell, "Photonic band-gap guidance in optical fibers", **282**, 1476-1478 (1998).
- [55] M. Humbert, J. C. Knight, G. Bouwmans, P. St. J. Russell, D. P. Williams, P. J. Roberts, and B. J. Mangan, "Hollow core photonic crystal fibers for beam delivery", *Opt. Express* **12**, 1477-1484 (2004).
- [56] T. T. Larsen, A. Bjarklev, D. S. Hermann, and J. Broeng, "Optical devices based on liquid crystal photonic bandgap fibres", *Opt. Express* **11**, 2589-2596 (2003).
- [57] J. Canning, E. Buckley, and K. Lytykainen, "Multiple source generation using air-structured optical waveguides for optical field shaping and transformation within and beyond the waveguide", *Opt. Express* **11**, 347-358 (2003).
- [58] A. Yariv, *Optical Electronics in Modern Communications*, Oxford University Press, New York (1997).
- [59] R. Ghosh, A. Kumar, and J. P. Meunier, "Waveguiding properties of holey fibres and the effective-V model", *Electron. Lett.* **35**, 1873-1875 (1999).
- [60] A. Sommerfeld, *Optics*, Academic Press, New York (1964).
- [61] T. M. Monro, D. J. Richardson, N. G. R. Broderick, and P. J. Bennett, "Holey optical fibers: An efficient modal model", *J. Lightwave Technol.* **17**, 1093-1102 (1999).
- [62] D. Mogilevtsev, T. A. Birks, and P. St. J. Russell, "Group-velocity dispersion in photonic crystal fibers", *Opt. Lett.* **23**, 1662-1664 (1998).
- [63] B. T. Kuhlmey, T. P. White, G. Renversez, D. Maystre, L. C. Botten, C. M. de Sterke, and R. C. McPhedran, "Multipole method for microstructured optical fibers. II. Implementation and results", *J. Opt. Soc. Am. B-Opt. Phys.* **19**, 2331-2340 (2002).
- [64] J. Arriaga, J. C. Knight, and P. St. J. Russell, "Modelling photonic crystal fibres", *Physica E* **17**, 440-442 (2003).
- [65] M. Qiu, "Analysis of guided modes in photonic crystal fibers using the finite-difference time-domain method", *Microw. Opt. Technol. Lett.* **30**, 327-330 (2001).
- [66] Z. M. Zhu and T. G. Brown, "Full-vectorial finite-difference analysis of microstructured optical fibers", *Opt. Express* **10**, 853-864 (2002).
- [67] D. Yevick and B. Hermansson, "Efficient beam propagation techniques", *J. Quantum Electron.* **26**, 109-112 (1990).
- [68] W. H. Press, B. P. Flannery, S. A. Teuklsky, and W. T. Vetterling, *Numerical recipes: the art of scientific computing*, Cambridge Univ., New York (1986).
- [69] S. Jungling and J. C. Chen, "A study and optimization of eigenmode calculations using the imaginary-distance beam-propagation method", *J. Quantum Electron.* **30**, 2098-2105 (1994).
- [70] T. A. Birks, D. Mogilevtsev, J. C. Knight, and P. St. J. Russell, "Single material fibres for dispersion compensation", *Proc. OFC'1999*, 108-110, paper FG2.
- [71] M. Koshiba and K. Saitoh, "Structural dependence of effective area and mode field diameter for holey fibers", *Opt. Express* **11**, 1746-1756 (2003).
- [72] G. P. Agrawal, *Nonlinear Fiber Optics*, Third edition, Academic Press, San Diego (2003).
- [73] F. Brechet, J. Marcou, D. Pagnoux, and P. Roy, "Complete analysis of the characteristics of propagation into photonic crystal fibers by the finite element method", *Opt. Fiber Technol.* **6**, 181-191 (2000).
- [74] M. D. Nielsen, N. A. Mortensen, M. Albertsen, J. R. Folkenberg, A. Bjarklev, and D. Bonacinni, "Predicting macrobending loss for large-mode area photonic crystal fibers", *Opt. Express* **12**, 1775-1779 (2004).
- [75] M. D. Nielsen, G. Vienne, J. R. Folkenberg, and A. Bjarklev, "Investigation of microdeformation-induced attenuation spectra in a photonic crystal fiber", *Opt. Lett.* **28**, 236-238 (2003).
- [76] R. R. Alfano and S. L. Shapiro, "Emission in the region 4000 to 7000 Å via four-photon coupling in glass", *Phys. Rev. Lett.* **24**, 584-587 (1970).
- [77] W. Lee Smith, P. Liu, and N. Bloembergen, "Superbroadening in H<sub>2</sub>O and D<sub>2</sub>O by self-focused picosecond pulses from a YAlG:Nd laser", *Phys. Rev. A* **15**, 2396-2403 (1977).
- [78] R. L. Fork, C. V. Shank, C. Hirlimann, R. Yen, and W. J. Tomlinson, "Femtosecond white-light continuum pulses", *Opt. Lett.* **8**, 1-3 (1983).

- [79] P. L. Baldeck and R. R. Alfano, "Intensity effects on the stimulated four photon spectra generated by picosecond pulses in optical fibers", *J. Lightwave Technol.* **5**, 1712-1715 (1987).
- [80] K. Mori, T. Morioka, and M. Sarumawatari, "Ultrawide Spectral Range Group-Velocity Dispersion Measurement Utilizing Supercontinuum in an Optical-Fiber Pumped by a 1.5  $\mu$ m Compact Laser Source", *IEEE Trans. Instrum. Meas.* **44**, 712-715 (1995).
- [81] J. C. Knight, J. Arriaga, T. A. Birks, A. Ortigosa-Blanch, W. J. Wadsworth, and P. St. J. Russell, "Anomalous dispersion in photonic crystal fiber", *IEEE Photonics Technol. Lett.* **12**, 807-809 (2000).
- [82] R. Holzwarth, T. Udem, T. W. Hänsch, J. C. Knight, W. J. Wadsworth, and P. St. J. Russell, "Optical frequency synthesizer for precision spectroscopy", *Phys. Rev. Lett.* **85**, 2264-2267 (2000).
- [83] A. V. Husakou and J. Herrmann, "Supercontinuum generation in photonic crystal fibers made from highly nonlinear glasses", *Appl. Phys. B-Lasers Opt.* **77**, 227-234 (2003).
- [84] S. Coen, A. H. L. Chan, R. Leonhardt, J. D. Harvey, J. C. Knight, W. J. Wadsworth, and P. St. J. Russell, "White-light supercontinuum generation with 60-ps pump pulses in a photonic crystal fiber", *Opt. Lett.* **26**, 1356-1358 (2001).
- [85] R. H. Stolen and C. Lin, "Self-phase modulation in silica optical fibers", *Phys. Rev. A* **17**, 1448-1453 (1978).
- [86] G. P. Agrawal, P. L. Baldeck, and R. R. Alfano, "Temporal and Spectral Effects of Cross-Phase Modulation on Copropagating Ultrashort Pulses in Optical Fibers", *Phys. Rev. A* **40**, 5063-5072 (1989).
- [87] R. H. Stolen, "Phase-matched-stimulated four-photon mixing in silica-fiber waveguides", *IEEE J. Quantum Electron.* **11**, 100-103 (1975).
- [88] N. Tzoar and M. Jain, "Self-phase modulation in long-geometry optical waveguides", *Phys. Rev. A* **23**, 1266-1270 (1981).
- [89] K. J. Blow and D. Wood, "Raman response function of silica-core fibers", *IEEE J. Quantum Electron.* **25**, 2665-2673 (1989).
- [90] R. H. Stolen, J. P. Gordon, W. J. Tomlinson, and H. A. Haus, "Raman response function of silica-core fibers", *J. Opt. Soc. Am. B* **6**, 1159-1166 (1989).
- [91] V. E. Zakharov and A. B. Shabat, *Sov. Phys. JETP* **34**, 62-69 (1972).
- [92] Y. Kodama and K. Nozaki, "Soliton Interaction in Optical Fibers", *Opt. Lett.* **12**, 1038-1040 (1987).
- [93] V. E. Zakharov and E. A. Kuznetsov, "Optical solitons and quasisolitons", *J. Exp. Theor. Phys.* **86**, 1035-1046 (1998).
- [94] W. Hodel and H. P. Weber, "Decay of Femtosecond Higher-Order Solitons in an Optical Fiber Induced by Raman Self-Pumping", *Opt. Lett.* **12**, 924-926 (1987).
- [95] P. Beaud, W. Hodel, B. Zysset, and H. P. Weber, "Ultrashort pulse propagation, pulse breakup, and fundamental soliton formation in a single-mode optical fiber", *IEEE J. Quantum Electron.* **23**, 1938-1946 (1987).
- [96] J. K. Lucek and K. J. Blow, "Soliton Self-Frequency Shift in Telecommunications Fiber", *Phys. Rev. A* **45**, 6666-6674 (1992).
- [97] F. M. Mitschke and L. F. Mollenauer, "Discovery of the soliton self-frequency shift", *Opt. Lett.* **11**, 659-661 (1986).
- [98] J. Santhanam and G. P. Agrawal, "Raman-induced spectral shifts in optical fibers: general theory based on the moment method", *Opt. Commun.* **222**, 413-420 (2003).
- [99] P. K. A. Wai, H. H. Chen, and Y. C. Lee, "Radiations by solitons at the zero group-dispersion wavelength of single-mode optical fibers", *Phys. Rev. A* **41**, 426-439 (1990).
- [100] N. Akhmediev and M. Karlsson, "Cherenkov Radiation Emitted by Solitons in Optical Fibers", *Phys. Rev. A* **51**, 2602-2607 (1995).
- [101] K. M. Hilligsøe, H. N. Paulsen, J. Thøgersen, S. R. Keiding, and J. J. Larsen, "Initial steps of supercontinuum generation in photonic crystal fibers", *J. Opt. Soc. Am. B-Opt. Phys.* **20**, 1887-1893 (2003).
- [102] K. M. Hilligsøe, T. V. Andersen, H. N. Paulsen, C. K. Nielsen, K. Mølmer, S. Keiding, R. Kristiansen, K. P. Hansen, and J. J. Larsen, "Supercontinuum generation in a photonic crystal fiber with two zero dispersion wavelengths", *Opt. Express* **12**, 1045-1054 (2004).
- [103] A. Proulx, J. M. Menard, N. Ho, J. M. Laniel, R. Vallee, and C. Pare, "Intensity and polarization dependences of the supercontinuum generation in birefringent and highly nonlinear microstructured fibers", *Opt. Express* **11**, 3338-3345 (2003).
- [104] P. A. Champert, V. Couderc, P. Leproux, S. Fevrier, V. Tombelaine, L. Labonte, P. Roy, C. Froehly, and P. Nerin, "White-light supercontinuum generation in normally dispersive optical fiber using original multi-wavelength pumping system", *Opt. Express* **12**, 4366-4371 (2004).
- [105] D. Derickson, *Fiber-Optic Test and Measurement*, Prentice Hall, (1998).

- [106] P. C. Becker, *Erbium-Doped Fiber Amplifiers Fundamentals and Technology*, Academic Press, San Diego (1999).
- [107] A. D. Galea, F. Couny, S. Coupland, P. J. Roberts, H. Sabert, J. C. Knight, T. A. Birks, and P. St. J. Russell, "Selective mode excitation in hollow-core photonic crystal fiber", *Opt. Lett.* **30**, 717-719 (2005).
- [108] T. von Lerber and M. W. Sigrist, "Cavity-ring-down principle for fiber-optic resonators: experimental realization of bending loss and evanescent-field sensing", *Appl. Opt.* **41**, 3567-3575 (2002).
- [109] K. Kasaya, O. Mitomi, M. Naganuma, Y. Kondo, and Y. Noguchi, "A simple laterally tapered waveguide for low-loss coupling to single-mode fibers", *IEEE Photonics Technol. Lett.* **5**, 345-347 (1993).
- [110] A. Mekis and J. D. Joannopoulos, "Tapered couplers for efficient interfacing between dielectric and photonic crystal waveguides", *J. Lightwave Technol.* **19**, 861-865 (2001).
- [111] T. Brenner and H. Melchior, "Integrated optical modeshape adapters in InGaAsP/InP for efficient fiber-to-waveguide coupling", *IEEE Photonics Technol. Lett.* **5**, 1053-1056 (1993).
- [112] P. Bienstman, S. Assefa, S. G. Johnson, J. D. Joannopoulos, G. S. Petrich, and L. A. Kolodziejski, "Taper structures for coupling into photonic crystal slab waveguides", *J. Opt. Soc. Am. B-Opt. Phys.* **20**, 1817-1821 (2003).
- [113] G. Chietera, A. H. Bouk, F. Poletti, F. Poli, S. Selleri, and A. Cucinotta, "Numerical design for efficiently coupling conventional and photonic-crystal waveguides", *Microw. Opt. Technol. Lett.* **42**, 196-199 (2004).
- [114] R. P. Kenny, T. A. Birks, and K. P. Oakley, "Control of optical fiber taper shape", *Electron. Lett.* **27**, 1654-1656 (1991).
- [115] T. A. Birks and Y. W. Li, "The shape of fiber tapers", *J. Lightwave Technol.* **10**, 432-438 (1992).
- [116] T. Alder, A. Stohr, R. Heinzlmann, and D. Jager, "High-efficiency fiber-to-chip coupling using low-loss tapered single-mode fiber", *IEEE Photonics Technol. Lett.* **12**, 1016-1018 (2000).
- [117] Z. Wang, B. Mikkelsen, B. Pedersen, K. E. Stubkjær, and D. S. Olesen, "Coupling between angled-facet amplifiers and tapered lens-ended fibers", *J. Lightwave Technol.* **9**, 49-55 (1991).
- [118] L. M. Tong, R. R. Gattass, J. B. Ashcom, S. L. He, J. Y. Lou, M. Y. Shen, I. Maxwell, and E. Mazur, "Subwavelength-diameter silica wires for low-loss optical wave guiding", *Nature* **426**, 816-819 (2003).
- [119] J. D. Love, W. M. Henry, W. J. Stewart, R. J. Black, S. Lacroix, and F. Gonthier, "Tapered single-mode fibers and devices 1: adiabaticity criteria", *IEE Proc.-J Optoelectronics* **138**, 343-354 (1991).
- [120] R. J. Black, S. Lacroix, F. Gonthier, and J. D. Love, "Tapered single-mode fibers and devices 2 experimental and theoretical quantification", *IEE Proc.-J Optoelectronics* **138**, 355-364 (1991).
- [121] I. Gutzow, T. Grigorova, and S. Todorova, "Kinetics of vitrification, glass relaxation and devitrification: a unified treatment", *J. Non-Cryst. Solids* **304**, 4-18 (2002).
- [122] A. H. Rose, "Devitrification in annealed optical fiber", *J. Lightwave Technol.* **15**, 808-814 (1997).
- [123] J. P. Laine, B. E. Little, and H. A. Haus, "Etch-eroded fiber coupler for whispering-gallery-mode excitation in high-Q silica microspheres", *IEEE Photonics Technol. Lett.* **11**, 1429-1430 (1999).
- [124] B. E. Little, J. P. Laine, and H. A. Haus, "Analytic theory of coupling from tapered fibers and half-blocks into microsphere resonators", *J. Lightwave Technol.* **17**, 704-715 (1999).
- [125] P. E. Barclay, K. Srinivasan, M. Borselli, and O. Painter, "Efficient input and output fiber coupling to a photonic crystal waveguide", *Opt. Lett.* **29**, 697-699 (2004).
- [126] P. E. Barclay, K. Srinivasan, and O. Painter, "Design of photonic crystal waveguides for evanescent coupling to optical fiber tapers and integration with high-Q cavities", *J. Opt. Soc. Am. B-Opt. Phys.* **20**, 2274-2284 (2003).
- [127] P. E. Barclay, K. Srinivasan, M. Borselli, and O. Painter, "Experimental demonstration of evanescent coupling from optical fibre tapers to photonic crystal waveguides", *Electron. Lett.* **39**, 842-844 (2003).
- [128] G. E. Town and J. T. Lizier, "Tapered holey fibers for spot-size and numerical aperture conversion", *Opt. Lett.* **26**, 1042-1044 (2001).
- [129] E. C. Mägi, P. Steinvurzel, and B. J. Eggleton, "Tapered photonic crystal fibers", *Opt. Express* **12**, 776-784 (2004).
- [130] J. K. Chandalia, B. J. Eggleton, R. S. Windeler, S. G. Kosinski, X. Liu, and C. Xu, "Adiabatic coupling in tapered air-silica microstructured optical fiber", *IEEE Photonics Technol. Lett.* **13**, 52-54 (2001).
- [131] D. Mogilevtsev, J. Broeng, S. E. Barkou, and A. Bjarklev, "Design of polarization-preserving photonic crystal fibres with elliptical pores", *J. Opt. A-Pure Appl. Opt.* **3**, 141-143 (2001).
- [132] H. M. Gibbs, *Optical Bistability: Controlling Light with Light*, Academic, Orlando, FL (1985).
- [133] K. Ikeda, "Multiple-valued stationary state and its instability of the transmitted light by a ring cavity system", *Opt. Commun.* **30**, 257-261 (1979).
- [134] D. Dangoisse, P. Glorieux, and D. Hennequin, "Chaos in a CO<sub>2</sub> laser with modulated parameters: Experiments and numerical simulations", *Phys. Rev. A* **36**, 4775-4791 (1987).

- [135] S. O. Konorov, D. A. Akimov, A. A. Ivanov, M. V. Alfimov, K. V. Dukel'skii, A. V. Khokhlov, V. S. Shevandin, Y. N. Kondrat'ev, and A. M. Zheltikov, "Cross-phase-modulation-induced instabilities and frequency shifts in a photonic-crystal fiber", *Appl. Phys. B* **80**, 437-439 (2005).

## Abstracts of publications

- [P1] G. Genty, M. Lehtonen, and H. Ludvigsen, "Effect of cross-phase modulation on supercontinuum generated in microstructured fibers with sub-30 fs pulses", *Opt. Express* **12**, 4614-4624 (2004).

*We investigate the effects of cross-phase modulation between the solitons and dispersive waves present in a supercontinuum generated in microstructured fibers by sub-30 fs pulses. Cross-phase modulation is shown to have a crucial importance as it extends the supercontinuum towards shorter wavelengths. The experimental observations are confirmed through numerical simulations.*

- [P2] G. Genty, M. Lehtonen, H. Ludvigsen, and M. Kaivola, "Enhanced bandwidth of supercontinuum generated in microstructured fibers", *Opt. Express* **12**, 3471-3480 (2004).

*Enhancement of the bandwidth of supercontinuum generated in microstructured fibers with a tailored dispersion profile is demonstrated experimentally. The fibers are designed to have two zero-dispersion wavelengths separated by more than 700 nm, which results in an amplification of two dispersive waves at visible and infrared wavelengths. The underlying physics behind the broad continuum formation is discussed and analyzed in detail. The experimental observations are confirmed through numerical simulations.*

- [P3] M. Lehtonen, G. Genty, M. Kaivola, and H. Ludvigsen, "Supercontinuum generation in a highly birefringent microstructured fiber", *Appl. Phys. Lett.* **82**, 2197-2199 (2003).

*We present experimental results on supercontinuum generation in a highly birefringent microstructured fiber. We show that such a fiber offers clear advantages for continuum generation over weakly birefringent fibers. In particular, the polarization is preserved along the fiber for all the spectral components. Furthermore, the two eigenpolarizations exhibit different dispersion characteristics, which provide a convenient way of tuning the properties of the generated continuum. We investigate the impact of the pump wavelength and pulse duration on the continuum and use the results to generate an ultrabroadband continuum extending from 400 to 1750 nm.*

- [P4] G. Genty, M. Lehtonen, and H. Ludvigsen, "Route to broadband blue light generation in microstructured fibers", *Opt. Lett.* **30**, 756-758 (2005).

*We explore theoretically the possibility of generating broadband blue light by copropagating a short soliton pump pulse and a broader signal pulse in a microstructured fiber with a zero-dispersion wavelength located between the center wavelength of the pump and the signal pulses. We show that the unique properties of microstructured fibers should allow for broadening of the signal pulse's spectrum by as much as a factor of 50 through the conjugate action of cross-phase modulation and a soliton self-frequency shift. The physical mechanism that leads to this large spectral broadening is analyzed by use of an extended nonlinear Schrödinger equation.*

- [P5] M. Lehtonen, G. Genty, and H. Ludvigsen, "Absorption and transmission spectral measurement of fiber-optic components using supercontinuum radiation", *Appl. Phys. B* **81**, 231-234 (2005).

*We report on broadband absorption and transmission measurements using supercontinuum sources generated in microstructured fibers. The advantages of the measurement technique include high brightness and broad bandwidth. Furthermore, the high spatial coherence of the supercontinuum source allows for efficient coupling into the device under test compared to standard light bulbs. Employing this technique, we measure the impurity absorption spectrum of Erbium-doped fibers with both low and high dopant concentration. The transmission spectra of a photonic bandgap fiber and a high-finesse fiber cavity are also characterized.*

- [P6] M. Lehtonen, G. Genty, and H. Ludvigsen, "Tapered microstructured fibers for efficient coupling to optical waveguides: a numerical study", *Appl. Phys. B* **81**, 295-300 (2005).

*We report on the possibility of using tapered microstructured fibers to improve the coupling efficiency from a standard single-mode fiber to a photonic crystal waveguide. The tapered microstructured fiber allows for reducing the mode mismatch between the output of the standard fiber and the input of the waveguide while maintaining single-mode guidance, which results in an enhanced coupling efficiency. Numerical simulations are conducted in order to optimize the cross-section of the microstructured fiber as well as the taper profile. An improvement of more than 4 dB is obtained compared to non-tapered fibers. For further improvement, an elliptical-core tapered microstructured fiber is analyzed. The effect of misalignment between the tapered microstructured fiber and the waveguide is also studied.*

- [P7] G. Genty, M. Lehtonen, and H. Ludvigsen, "Optical bistability and signal processing in a microstructured fiber ring resonator", *Appl. Phys. B* **81**, 357-362 (2005).

*We explore theoretically the effects of bistability in a microstructured fiber-based ring resonator. Numerical simulations indicated that bistable behavior of the fiber cavity can be observed with a short length of fiber. Feasibility of all-optical processing using this type of cavity is also investigated. In particular, we show that a ring cavity including a microstructured fiber should allow to perform flip-flop and time-division demultiplexing functions. The analysis presented here will be useful for future design of bistable microstructured fiber device.*



ISBN 951-22-7913-4  
ISBN 951-22-7914-2 (PDF)  
ISSN 1795-2239  
ISSN 1795-4584 (PDF)